Astrophysics & Geophysics:

Based on the space-time of String theory exploring dark matter inside the Earth

Newidea Research Center

Hsien-Jung Ho

Website： http://newidea.org.tw

E-mail： newidea.ufoho@msa.hinet.net

Background:

Master Degree, 1969 / Civil Engineering Department, National Cheng Kung University

Experience:

Associate professor / Ming-Hsin University of Science and Technology

Associate researcher / Industrial Technology Research Institute of Taiwan

Chief of A & D Section, BES Engineering Corporation

Chairman & Honorary Chairman / Taiwan Ufology Society

Speaker of Popular Science / National Taichung Library

Speaker of Popular Science / National Taiwan Education Center

Consultant of School Administration / National Changhua Senior High School

Chairman / Ping Sung Industrial Corporation

Host / Newidea Research Center

Address: 10 Fl., No. 110-6, Jie-Shou N Road, Changhua City, 50060, Taiwan

Other writings of paper:

Ho, Hsien-Jung, 1993. Reconstruction of the Earth Model and Discovery of the Interior Dark Matter, *First Symposium on UFO cross-strait. China Ufology Institute.* http://newidea.org.tw/PDF/S2.pdf.

Ho, Hsien-Jung and Hsui, Peter, 2005. Mega-Tsunami In Northeastern Taiwan At Least 12,000 Years Ago, *3rd International Conference On Asian and Pacific Coasts 2005,* Hanrimwon Publishing Co. Seoul Korea, 199-208. http://newidea.org.tw/PDF/S4.pdf.

ABSTRACT

The dark matter puzzles scientists for more than 80 years, until now still no solution. Apply the String theory, which has the characteristics of ten-dimensional space-time, to solve the problem. According to “Causality Principle” and “Anthropic Principle”, the full Universe may be divided into triple Universes, and the dark matter should be taken as a terrestrial planet in other space than ours. The best method of exploring dark matter is to start from the Earth where we live. According to the characteristics of the Earth's interior, equitably examining its constitution, temperature, density and pressure from a different view of the core, the special arguments are put forward. It is inferred that the solid rock and the magma change states interactively at the CMB. In the low viscosity F-layer of outer core, high temperature causes some elements and oxides of magma to undergo oxidation-reduction reactions and separate due to its gravity. The great amount of heats, produced from radiogenic heat, chemical reaction heat and nuclear fission heat, become the power sources for the geo-dynamo of great convection cell, which are the flows of the magma and the solid rock migrating up to the crust and down across the CMB to the F-layer. Based on the new conception and applying a simplified method tries the different density distribution curves of 4 models in the core to calculate the data of the Earth, and compared with the existing current data of the Earth. The insufficient mass and moment of inertia are the missing matters, which are taken as the parts of dark matter, which may be in the interior of the Earth. Apply the simplified method to evaluate the Earth's mass and moment of inertia that are found to be only 85.73% and 94.82% of the current data. By the two insufficiencies of the Earth's data, formulating the reasonable assumptions, a planet of dark matter inside the earth has been figured out. And then calculate gravity and pressure in every depth within the Earth to check suitability or not. Finally a dark matter, radius 3700.375 km planet about 1.33 times of Mars, is reasonably inside the Earth but other space than ours. The new Earth model may be confirmed from Chandler wobble, and some great scientific problems, such as: dark matter, dark energy and composition of the Earth, etc., have been roughly solved.

Key Words: Density jump, Convection cell, Chandler wobble, Dark matter, Dark energy, 10-Dimensional space-time theory, Multiverse.

1. Introduction

Zwicky (1937), Caltech astronomer, noticed that masses of nebulae were estimated either from the luminosities of nebulae or from their internal rotations, both methods of determining nebulae masses are unreliable. He surmised that the Coma cluster of nebulae was moving around so fast that some extra, hidden mass must be present to supply the gravitational glue.

In the 1970s, astronomers detected that when star outside edges of the Milky Way and other spiral galaxies were found to be orbiting faster than theory predict; individual galaxies, it seemed, also harbored a reservoir of unseen matter whose gravity kept their stars from escaping [Bartusiak, 1988]. The total mass of stars in a galaxy, which can be estimated by observing the galaxy with an astronomical telescope, is less than

10% of this total mass of the galaxy estimated from the orbiting stars. The phenomenon appears throughout the Universe. Unobservable matter, amounted to more than 90 % mass of the entire Universe, is called dark matter [Stsrobinskii & Zel'dovich, 1988]. The dark matter is real that can only be detected by its gravitational influence on visible matter. While almost all astronomers agree on the existence of the dark matter; however, after more than 8 decades of search, there is nothing gained. Therefore, the dark matter is a major problem, which still has no solution.

In 1998, the High-Z Supernova Search Team published observations of type 1a supernova as standard candles [Riess *et al.*, 1998], and in 1999 the Supernova Cosmology Project followed immediately [Perlmutter *et al.*, 1999], then the two independent projects obtained results suggesting a totally unexpected acceleration in the expansion of the Universe. In order to explain the phenomenon of the Universe is expanding at an accelerating rate, "dark energy" is the most accepted hypothesis to the observations. Dark energy acts as a sort of an anti-gravity and is responsible for the present-day acceleration of the Universal expansion.

In 2012, the Wilkinson Microwave Anisotropy Probe (WMAP) has refined its measurements with a final data of the present-day Universe: 4.63% normal (baryonic) matter, 23.3% dark matter and 72.1% dark energy [Bennett *et al.*, 2013]. In 2014, the Planck Cosmology Probe released the new estimated content of dark matter 26.8 %, dark energy 68.3 % and normal matter 4.9 % in the Universe [Ade *et al*., 2014]. Roughly there are dark energy 68%, dark matter about 27%, and the rests — everything ever observed with all of our instruments and all normal matter — add up to less than 5% in the Universe.

Sawangwit and Shanks (2010), astronomers in the Physics Department at Durham University, used astronomical objects that appear as unresolved points in radio telescopes to test the way the WMAP telescope smoothed out its maps. They find that the smoothing is much larger than previously believed, suggesting that its measurement of the size of the CMBR (Cosmic Microwave Background Radiation) ripples is not as accurate as was previously thought, which in turn makes the standard model of the Universe open to question. If true this could mean that the ripples are significantly smaller, which could imply that dark matter and dark energy are not present after all.

Dark energy is a current scientific hypothesis, being neither matter nor radiation, its physical properties have no any clue, and we don't know how it works, and dark matter is also no solution, so, now all astrophysicists take them as the major problems.

2. Ten-dimensional space-time of String theory reveals multiverse

In order to address these questions of astrophysics, in 1970s String theory was introduced. There are two theoretical framework in String theory: one is called Superstring theory [Schwarz & Scherk, 1974] that requires 10 space-time dimensions, and the other is called M-theory [Witten, 1995, 1998] that originates from a more fundamental 11-dimensional theory.

The origin of String theory is based on the Universe constitution of nine-dimensional space and one-dimensional time. String theory has been strictly proved a mathematical theory that is currently the only one can unify the four fundamental forces of nature, and potentially provides a unified description of gravity and

particle physics.

The starting point for String theory is the idea that the point-like particles of particle physics can also be modeled as one-dimensional objects called strings. The characteristic length scale of strings is assumed to be on the order of the Planck length, or 10^{-35} meters that looks just like an ordinary particle, with its mass, charge, and other properties determined by the vibrational states of it in different ways. One notable feature of String theories is that these theories require extra dimensions of space-time for their mathematical consistency. The 10-dimensional space-time of the String theory is interpreted as the product of ordinary 4-dimensional space-time and a 6-extra-dimensional spaces, which is as yet unobserved [Scherk & Schwarz, 1975].

String theory is now not established as well as Relativity theory, because there is no the exact boundary condition to fit the real Universe and works out a theoretically solid basic geometry, though many mathematicians and physicists have attempted to compactify the constitution of ten-dimensional space-time model through spontaneous symmetry breaking, to a four-dimensional one as our known world and 6-extra-dimensional space, which is compacted to be tiny space called Calabi-Yau space as Plank space (10^{-35} m), but no proposed method meets perfection.

In the multidimensional theories of String theory, the force of gravity is the only force of nature with effect across all dimensions. This explains the relative weakness of gravity compared to the other forces of nature (as electromagnetic wave) that cannot cross into extra dimensions. In that case, dark matter could exist in extra dimensions that only interact with the matter in our space through gravity. That dark matter could potentially aggregate in the same way as ordinary matter, forming extra-dimensional galaxies [Siegfried, 1999]. To date, no experimental or observational evidence is available to confirm the existence of these extra dimensions.

Dvali (2004) suggested that the extra dimensions of space does not curl up (not compactified) becomes minimum, but infinite in size and uncurved, just like our ordinary three-dimensional view. Character in String theory, they rethink the "extra dimension" problem, that is, gravity can roam to an additional dimensions of space. They think that the accelerated expansion of the Universe is not caused by dark energy, but because gravity leaks out of our world. In particular, the theory predicts that the Universe has extra dimensions into which gravity, unlike ordinary matter, may be able to escape. This leakage would warp the space-time continuum and cause cosmic expansion to accelerate. Thus the extra dimensions need not be small and compactify, but may be large extra dimensions; i.e., outside our ordinary three-dimensional space, there are the same six extra dimensions of space in the Universe.

Without breaking the nine-dimensional space of the Universe down, the ten-dimensional space-time is considered to universally exist. According to “Causality Principle”, an effect cannot occur before its cause, which means time has a direction and cannot be divided into some different parts. So one-dimensional time is taken as a common standard in order of event in the Universe. According to “Anthropic Principle”, which is the simple fact that we live in a Universe set up to allow our existence. It means that three-dimensional space and one-dimensional time are taken as one Universe as our living world. Therefore, the nine-dimensional

space can be divided into three portions, and each portion has a common standard time. It mean there are three-cosmic framework in the Universe, called multiverse or triple Universes, which cannot be observed directly with one another.

In 2002, the Planck space map of cosmic background radiation shows a stronger concentration in the south half of the sky and a ‘cold spot’ that cannot be explained by current understanding of physics. In 2005, Laura Mersini-Houghton, theoretical physicist at the University of North Carolina, and Richard Holman, professor of Carnegie Mellon University, predicted that anomalies in radiation existed that can only have been caused by the gravitational pulling on our Universe from other Universes as it formed during the Big Bang [Woit, 2013]. It is the first 'hard evidence' that other universes exist has been found by scientists, and it accords with the three-cosmic framework of the Universes.

In 1957, Princeton University Dr. Everett (1957) devised “the many-worlds interpretation (MWI) of quantum mechanics”. The core of the idea was to interpret in the quantum world, an elementary particle, or a collection of such particles, can exist in a superposition of two or more possible states of being. An electron, for example, can be in a superposition of different locations, velocities and orientations of its spin. Yet anytime scientists measure one of these properties with precision, they see a definite result—just one of the elements of the superposition, not a combination of them. Nor do we ever see macroscopic objects in superposition. The many-worlds interpretation is a theory of multiple Universes [Byrne, 2008].

Most cosmologists today accept this type of multiple Universes. According to String theory, the three-cosmic framework of the Universes have characteristics in which each Universes describes a world of general matter and the others describe another world, which we know nothing. Among any another worlds, there is no basic interactive forces of nature except gravity; in other words, the theoretic graviton in the field of gravity can penetrate all three Universes; however, the light (electromagnetic wave) cannot that means the dark matter may be situated in a Universes other than ours. The best method of exploring dark matter is to start from the Earth where we live.

3. Based on the multiverse exploring dark matter from the Earth

In the current Earth model utilized in seismological investigations, such as body-wave travel times, surface-wave dispersion and free oscillation periods for researching the chemical composition and the density distribution of the Earth, the portions of the crust and the upper mantle have been analyzed with satisfactory accuracy. Regarding the lower mantle and the core portion, however, there remain a number of questions to be answered. It has been well known that there are two convections circulating individually below the crust to the lower mantle and in the outer core itself. The mantle and the core are not in chemical equilibrium and the fine structure of the core-mantle boundary (CMB) is not well understood. Although some hypothesizes such as the existence of a D″ layer in the lower mantle and iron combined with oxygen as the primary alloying constituent of the outer core are suggested, and a lot of advances of this research have come out, but there are also some discrepancies in the interior of the Earth [Creager & Jordan, 1986; Morelli & Dziewonski, 1987]. Furthermore, there is no conclusive evidence that the inner core is in thermodynamic equilibrium with the

outer core. The main problem is a lack of phase equilibrium data for plausible core compositions at the appropriate conditions, added to the fact that seismological observations do not yet offer a decisive constraint on the difference in composition between the inner and outer core [Jeanloz, 1990]. In order to investigate the outer core, a different view of the deep interior of the Earth should be taken to analyze the Earth's constitution, composition, temperature and pressure, and a revolution in the chemical composition should be developed.

3.1 The arguments at the core mantle boundary

With regard to the Earth's interior, the constitution of the deep interior is uncertain with some difficulties. In order to conduct further investigation, the Preliminary Reference Earth Model (PREM) [Dziewonski & Anderson, 1981] is taken as the current Earth model in this paper. At the CMB of this model, the solid portion of the lowermost mantle has a density of 5.57 g/cm^3, which jumps to 9.90 g/cm^3 in the liquid portion of the top core, a density jump of 77.74 %. However, in the PREM the density jumps significantly at the CMB, all investigations cannot confirm the data directly, so, research about the interior constitution of the Earth is needed, especially at the CMB.

Deducting the certain quantities of the crust and the mantle portion from the known data of the mass and the moment of inertia of the Earth, there are the great amounts of rest values. In order to match it, the ordinary way is to set a distribution of high density in the core and also a high density jump at the CMB. The reason is considered as a matter of course within the domain of current science. If the factor is not initially taken into consideration, a different conclusion may be drawn. There are some arguments in the topic of the CMB as follows:

1. Ramsey (1948) and Lyttleton (1973) have challenged the concept of an iron core. They suggest that the silicates (iron silicates and magnesium silicates) are the main composition of the mantle. Because the solid mantle under high temperature and high pressure at the CMB, the mantle silicates undergo phase-changes, which are called Ramsey's phase-changes, a solid phase changing into a liquid phase in the top core, to produce the material of high density, low melting point and electrical conductivity. Ramsey's hypothesis is still accepted by a few geophysicists for several reasons.

2. Knopoff (1965) showed that cross a phase transition near the surface of CMB, one can predict that the bulk modulus K increases by the increasing of the density ρ; in such a way, the ratio K/($\rho^{7/3}$) is kept constant. From the models, the bulk modulus remains essentially unchanged across the CMB that is difficult to account for a large density jump from about 5.57 g/cm^3 to about 9.90 g/cm^3 in the PREM. On this basis, it is difficult to argue in favor of the density distribution to be smoothly continuous at the CMB and the composition of outer core is silicates.

3. Buchbinder (1968) studied the variation in amplitude, with an epicentral distance Δ, of the reflected phase PcP. Calculations of reflection coefficients at a plane solid-liquid boundary show that a model with *P* and *S* velocities at the bottom of the mantle of 13.64 km/sec and 7.30 km/sec, respectively; with a *P* velocity at the top of the core of 7.5 km/sec; and with a ratio of core density to mantle density of 1.0 will satisfy the observations of amplitude and change of initial phase of *PcP*. A range of similar models with velocities at the

top of the core down to 7.2 km/sec and density ratios as high as 1.05 will also satisfy the observations. He found that the amplitude-distance curve, which displays a minimum at $\Delta = 32°$, was not consistent with the computed reflection amplitudes for a solid-liquid interface, if the previously accepted values of *P* velocity and density were employed. A model is proposed that is consistent with the observed amplitudes, provides no discontinuity in density between the low mantle and the core. Amplitude observations of *PKKP* phases also satisfy the model. Such a model may arise if there is considerable mixing of the core material with the lowermost mantle, and vice versa.

From the items of 1, 2 and 3 above, the descriptions can be initially identified that the materials of mantle and core mixing with each other, and the density distribution between the lower mantle and the outer core should be continuity in order to solve some problems in the geophysics. The main composition of the outer core should be considered as the same ingredients of molten rock and/or mineral silicates, which are chemically consistent with the same ingredients of the lowermost mantle, and maybe not liquid iron.

Iron is the richest nature metal element in the Universe. Because of the Earth's interior mass, density distribution and average density, it is needed an iron element to explain the composition of the core. However, this does not mean that we have proved that the core is made of "iron" parts. The materials of mantle and core based on "Birch Diagram" [Birch, 1939], which was inspected the relations of "velocity/density" in each element, to indicate the composition of matter. These claims are the Earth Sciences today on the "golden rule". By "Birch Diagram" speculated that the core is mainly composed of "iron", but that's just an assumption, we cannot examine it [Liu, 1974].

The composition of the Earth by the proportion of the meteorites that fall to the ground, can be found the more stone meteorites on Earth, iron meteorite contains only about 15%. The planet Earth basically gathered from small particles of the same cold solid ingredients, therefore did not at any stage possibly in the interior of the Earth to develop into an iron core. If by the primary reference earth model (PREM) calculate the mass of iron core part of the Earth that is about one-third of the Earth’s. It is share of iron meteorite much large than the iron meteorite containing 15%, apparently not reasonable. So, does the core, particularly the part of liquid outer core, fills with iron? It is worth exploring. So, the outer core need not be filled with iron, perhaps as the mantle may be mineral silicates.

3.2 Topography of CMB reveals both sides at CMB to be the same materials

A sufficient quantity of high-quality digital data from two global networks: a network for very long period seismology [Agnew *et al*., 1976] and the seismic research observatory [Peterson *et al*., 1976] began operation in the mid-1970s and developed about three decades provided the framework of formal analysis, and the availability of computers, made feasible the handling of immense amounts of data and the large-scale calculations necessary in three-dimensional problems. Geophysicists recorded on Earth more than 15,000 times magnitude 4.5th-class earthquake data, input seismic laboratory computer, drawing the three dimensional topographical map of the Earth's Interior, and computer tomography X-ray photograph, produced the CMB topography, which is found in boundary of solid mantle and liquid outer core. The undulations of

CMB in regions from 3,000 km to 6,000 km, denote the irregular high mountains and deep valleys. The amplitude of the boundary is ±6 km, in other word, the height difference more than 10 kilometers, even higher than the world's highest peak──Mount Everest, and in a very unstable state [Morelli & Dziewonski, 1987].

In three-dimensional maps, tomographic models represent an instantaneous, low-resolution image of a convection system. Detailed interpretation knowledge of mineral and rock properties as yet poorly known that are required. Maps of CMB topography have been derived on the basis of seismological inversions of longwave travel-times to construct three-dimensional maps with the magnitude of amplitudes from ±3 km up to ±6 km (relief 12 km) and with 3000～6000 km scale lengths (e.g., Creager & Jordan, 1986; Gudmundsson *et al.*, 1986; Morelli & Dziewonski, 1987; Doornbos & Hilton, 1989; Forte & Peltier, 1991; Neuberg & Wahr, 1991; Rodgers & Wahr, 1993; Obayashi & Fukao, 1997; Boschi & Dziewonski, 1999, 2000; Garcia & Souriau, 2000; Sze & van der Hilst, 2003; Yoshida, 2008; Steinberger & Holme, 2008; Soldati *et al.*, 2013, 2014). The CMB topography is different from that predicted by the hydrostatic equilibrium theory and exceeds the inferences from geodesic studies.

In order to reduce the amplitudes of CMB topography, several subsequent studies (e.g., Forte *et al.*, 1995*;* Steinberger & Holme, 2002, 2008) implied that the radial viscosity decrease adjacent to CMB, and some study addressed the effects of several factors (notably lateral viscosity variations in the mantle, dense piles, and the low-viscosity D″ layer) on CMB topography to get the same effect that they suggested smaller peak amplitudes of ±1.5 km (e.g., Doornbos, 1978; Hager *et al*., 1985; Bowin 1986; Gwinn *et al*., 1986; Rodgers & Wahr, 1993; Earle & Shearer, 1997; Garcia & Souriau, 2000; Koper *et al.*, 2003; Yoshida, 2008*;* Tanaka, 2010) to fit the general knowledge of geoscience, all as following table 1. If we doesn't address the effects on CMB topography to get the smaller peak, the amplitudes of CMB topography should be large than ±5 km, so, the relief of 10 km is taken as an average value to discussion.

Table 1. Summary of some methods for studying the CMB topography [Schlaphorst *et al*., 2016]

Study	Method / seismic phases	Topography amplitude
Doornbos (1978)	PKP precursors	± few 100 m
Hager *et al*. (1985)	Geoid modelling	±1.5 km
Bowin (1986)	Inversion	±1.5 km
Gwinn *et al*. (1986)	Geodetic nutation observations	±0.5 km
Morelli & Dziewonski (1987)	PcP, PKPbc	±6 km
Neuberg & Wahr (1991)	PcP PcP, PKPab PKPbc, PKPdf	±3 km ±10 km, ±30 km
Earle & Shearer (1997)		±0.35 km
Garcia & Souriau (2000)		±4 km
Sze & van der Hilst (2003)	PcP, PKPab, PKPbc, PKKPab, PKKPbc PKPdf	±5 km ±13 km
Yoshida (2008)	Numerical modelling	±8 km
Steinberger & Holme (2008)	Mantle flow model	±3 km
Tanaka (2010)	PcP, P4KP	±2 km

A complex set of constraints on the possible modes of convection in the earth's interior has not yet been

worked out; this will require numerical modeling of convection in three dimensions. Thus the interpretation of the geographical information from seismology in terms of geodynamical processes is a matter of considerable complexity [Woodhouse & Dziewonski, 1989]. The topography on the CMB can be sustained only by dynamic processes, and these processes must be crucially understood. Despite the general agreement on the overall shape of CMB undulations, these details of the peak-to-peak amplitude and pattern are still debated [Soldati *et al*., 2014]. Geoscientists used PcP, PKPbc, and PKKPbc phases selected from the data set by Engdahl *et al*. (1998) and concluded that CMB topography cannot be resolved [Sze & van der Hilst, 2003]. At present, consensus regarding the regional pattern of the CMB topography, as well as on its peak-to-peak amplitude is lacking [Koelemeijer *et al*., 2012].

Bloxham and Gubbins (1987) argued that flow near the core surface may be controlled by lateral temperature variations in the lowermost mantle, which are amply sufficient for this to be a significant effect. But Stevenson (1987) inferred the lateral temperature variations near the outer core surface are very small, amounting to only a few millikelvin, based on $\alpha = 5\times10^{-6}K^{-1}$ (α is coefficient of thermal expansion). The lateral temperature variations are so small that it should not affect the flow near the core surface, and the pattern of topography of the core-mantle boundary are determined by processes in the core [Morelli & Dziewonski, 1987].

An approximate analysis is given for the likely fractional lateral density variations ($\delta\rho/\rho$) in the outer core, caused by large scale-length fluid dynamical processes. It is first shown that fractional density and fractional seismic velocity variations are probably comparable, so that fluid dynamic arguments have relevance to seismic data. In regions of nearly neutral stability in the outer core, an analysis of convective vigor indicates an upper bound of $|\delta\rho/\rho| \leq 10^{-8}$. Scientists undertaking analysis of the Earth's seismic travel times or normal modes can safely assume that there are negligible lateral variations in the outer core [Stevenson, 1987].

According to the PREM, iron is the major component of the core, and there is a density jump of 77. 74 % at the CMB. Neglecting the gravity anomaly, the pressure of lateral difference at the lowermost level of the CMB is 4.246 kbar considering a relief height of only 10 km. This pressure can produce an increasing iron density of 6.323×10^{-3} g/cm^3 under conditions at the top of core, and yields a fractional lateral density variations of $\delta\rho/\rho = 0.639\times10^{-3}$, which is far beyond the upper bound of fractional lateral density variations 10^{-8} [Morelli & Dziewonski, 1987].

In three-dimensional maps of the Earth's interior, the topography of the CMB is different from that predicted by the hydrostatic equilibrium theory, which contains information important to geodynamic processes and the geomagnetic secular variation. The topography on the CMB is likely to result from convection in the overlying mantle [Young & Lay, 1987]. Ruff and Anderson (1980) argue for dynamo action in the core maintained by differential heating of the core by the mantle, and some agreements of that are probably determined by processes in the core [Bloxham & Jackson, 1990]. The depressed regions of the topography are dynamically supported by down welling of cool mantle material [Gudmundsson *et al*., 1986;

Lay, 1989]. Obviously the relief is dynamically supported and provides coupling between the solid mantle and the fluid core.

The scientists undertaking analysis of the Earth's geoid or seismic travel times or normal modes can safely assume that there are negligible lateral density variations in the outer core. The lateral density differences in the top of outer core are so small that it could not provide a relief in excess of 10 km at the CMB, which is related to mantle temperature, and suggest further effects due to topography associated with subduction slabs, and may have a mechanical rather than thermal effect on the flow [Gubbins & Richards, 1986].

It is obviously in terms of the geodynamic processes that only the vertical interactions of material and the temperature between the lowermost mantle and the outer core are the main cause. In order to maintain the 10 km of relief, the density difference between the liquid state and the solid state at the CMB must be very small. There is a significant suggestion that the density of the materials between the both sides at the CMB must be similar or equal; i.e., the hypothesis that the same materials between a solid mantle and a liquid core change states with each other at the CMB to produce topography of the CMB more than 10 km relief.

Therefore, the density jump of 77.74 % at the CMB of the PREM may be considered as an unreasonable basis of reference. Thus based on the topography, the idea of a spherical structure of the CMB in the Earth model has been challenged. Therefore, a new study is necessary to determine the actual Earth’s model.

3.3 The great convection cell spanning the crust through F-layer

In 1971, geophysicist Morgan (1971) proposed the hypothesis of mantle plumes, which generated from thermal boundary layers have been invoked for decades to explain the formation of hotspots and flood basalts provinces on the Earth. In this hypothesis, convection in the mantle transports heat from the core to the Earth's surface in thermal diapirs. There are two largely independent convective processes occur in the mantle. 1. *Mantle plumes*, which carry heat upward in narrow, rising columns, driven by heat exchange across the core-mantle boundary to the crust. 2. The broad convective flow associated with *plate tectonics*, which is driven primarily by the sinking of cold plates of lithosphere back into the mantle [Morgan, 1972].

The interior heat gives rise to convection currents in the Earth's mantle, energized by the heat emitted by the core. Various lines of evidence have been cited in support of mantle plumes. Plate tectonics is a scientific theory describing the large-scale motion of Earth's lithosphere. Tectonic plates builds on the concept of continental drift, and has be accepted by the geoscientific community after seafloor spreading was validated.

Mantle plumes are tubes of hot rock rising from Earth's core, many of them underneath known volcanic hot spots at Earth's surface. The plumes are fatter than expected, which means that they carry more heat away from Earth's core, an indication that plumes are important for cooling the planet of Earth [Hand, 2015].

Earth's internal heat powers most geological processes and drives thermal plumes through convection or large scale upwelling and doming. However, no plume has yet been found to satisfy all the criteria currently attributed to plumes, adding that the hypothesis has become too flexible, with ad hoc variations tacked on to accommodate any finding [Puchkov, 2009]. It is still unresolved whether features that have been attributed to

plumes are primarily the result of plate tectonics and stress, or fluid dynamics and high temperature, and the factors of plate movement is unclear, and still the subject of much debate. With uncertainty in the areas of lower mantle and outer core, and possible unrecognized complexity, precision in the estimates of CMB heat flux is not yet clearly in hand.

The heat loss from the Earth's surface is more than the heat getting from the Sun. If the core does not for the continued release of heat, the Earth would have cooled off and become a dead rocky globe like as Mars or Moon. Releasing heat as we know is by the nuclear energy from the much slower decays of radioactive elements like as ^{238}U, ^{235}U, ^{232}Th, and ^{40}K [Van Schmus, 1995], gradually, however, radiogenic heating generated in the core turns the iron into a convecting geo-dynamo that maintains a magnetic field strong enough to shield the planet from the solar wind. This heat leaks out of the core into the mantle, causing convection in the rock that moves crustal plates and fuels volcanoes.

In 1997, it became possible that using seismic tomography to image submerging tectonic slabs penetrating from the surface all the way to the core-mantle boundary [Kerr, 1997]. Hotspots power the volcanic activity that is continuing to produce basalt-lava, which forms the Hawaiian Islands and Iceland. Norwegian scientists discovered that basalt eruptions in the Hawaiian Islands and in Iceland varied significantly over time [Mjelde & Faleide, 2009]. Seismic tomography appears to image vertical, column-like heat paths extending to the edge of the core for each of those hotspots. As the two hotspots are located on opposite sides of the globe, Mjelde, Wessel and Müller (2010) suggest the co-pulsations are a global hotspot phenomenon that appears to represent changes in heat from the Earth's core.

The current total heat flow at Earth's surface estimates to be refined and are agreeing at around 43–49 TW (terawatts) [Pollack *et al.*, 1993; Jaupart *et al.*, 2007; Lay *et. al.*, 2008; Davies & Davies, 2010; Davies, 2013], involves contributions from secular cooling, radiogenic heating from decay of ^{238}U and ^{232}Th, heat entering the mantle from the core, and various minor processes such as tidal deformation, chemical segregation and thermal contraction. Most models assume a CI carbonaceous chondrite origin for the Earth, leading to a total heat production in the silicate Earth (mantle plus crust) of about 20 TW [Javoy, 1999], estimates of mantle primordial heat loss range between 7 and 15 TW [Dye, 2012]. The heat flow across the CMB cannot be greater than 29 TW, a value obtained in the case of a steady mantle temperature.

The radioactive power of the planet is predicted a range of radioactive powers, overlapping slightly with the other at about 24 TW, and together spanning 14–46 TW. Approximately 20% of this radioactive power (3–8 TW) escapes to space in the form of geo-neutrinos. The remaining 11–38 TW heats the planet with significant geodynamical consequences, appearing as the radiogenic component of the 43–49 TW surface heat flow. The non-radiogenic component of the surface heat flow (5–38 TW) is presumably primordial, a legacy of the formation and early evolution of the planet [Dye, 2012].

Intimately related to terrestrial radiogenic heating is a flux of electron antineutrinos, commonly called geo-neutrinos [Fiorentini *et al.*, 2007]. Beta decays of daughter nuclides in the radioactive series of ^{238}U and ^{232}Th produce detectable geo-neutrinos. Geo-neutrino observatories lead to estimate the radiogenic heat

production. Geo-neutrino observatories operate underground at two Northern Hemisphere locations in Japan [Gando *et al.*, 2011] and Italy [Araki *et al.*, 2005; Bellini *et al.*, 2010], monitor large volumes of organic scintillating liquids for the delayed coincidence signal, indicative of electron antineutrino quasi-elastic scattering on protons. Existing observations with limited sensitivity to geo-neutrinos from the interior of Earth constrain radiogenic heating to 15–41 TW [Dye, 2012], assuming a thorium-to-uranium abundance ratio (Th/U = 3.9) and a homogeneous mantle. The radiogenic heating of 15–41 TW is very close to the predicted range of 14–46 TW.

Nuclear energy generated in the core from the radioactive elements not only slower decay but also faster fission. Kuroda (1956) applied Fermi's nuclear reactor theory [Fermi, 1947] and demonstrated the feasibility that seams of uranium ore could engage in neutron-induced nuclear fission chain. In 1972, French scientists Francis Perrin discovered the intact remains of a natural nuclear fission reactor in a uranium mine at Oklo, in the Republic of Gabon, that had operated just as Kuroda had predicted. Oklo is the only known location for this in the world and consists of 16 sites at which self-sustaining nuclear fission reactions took place approximately 1.7 billion years ago [Hagemann & Roth, 1978; Meshik *et al.*, 2004]. Oak Ridge National Laboratory used computer programs to calculate the operation of different types of nuclear fission reactors that showed the geo-reactor would function as a fast neutron breeder reactor over the entire existing time of the Earth [Hollenbach & Herndon, 2001].

Geomagnetic field reversals and changes in intensity are understandable from an energy standpoint as natural consequences of intermittent and/or variable nuclear fission chain reactions deep within the Earth. Moreover, deep-Earth production of helium, having $^{3}He/^{4}He$ ratios within the range observed from deep mantle sources, is demonstrated to be a consequence of nuclear fission. Numerical simulations of a planetary-scale geo-reactor were made by using the SCALE sequence of codes. The results clearly demonstrate that such a geo-reactor near or at the center of the Earth would function as a fast-neutron fuel breeder reactor; and would function in such a manner as to yield variable and/or intermittent output power. [Hollenbach & Herndon, 2001].

Geo-reactor-heat produced by nuclear fission can be variable, unlike heat from the natural decay of long-lived radioactive isotopes, which is essentially constant, decreasing slightly over very-long periods of time. Antineutrino measurements to date have not refuted the existence of the geo-reactor, but set an upper limit of 3 TW on its energy production [Gando *et al.*, 2011] that does not include the contribution from radioactive decay energy of the geo-reactor's associated uranium.

As previous statements, the core is the most abundant in heat flow that part of it is thought to represent power dissipated by the geo-dynamo, and to produce the geomagnetic field [Gubbins & Masters, 1979]. A nuclear fission geo-reactor is clearly an acceptable alternative energy sources, and its output can be variable and/or intermittent, a fact that is quite consistent with the observed variability of the geomagnetic field [Hollenbach & Herndon, 2001]. Heat flow from the core is necessary for maintaining the convecting outer core and the geo-dynamo and Earth's magnetic field, therefore primordial heat from the core enabled Earth's

atmosphere and thus helped retain Earth's liquid water [Korenaga, 2008].

At least some of the 2 million cubic kilometers of lava which spread over parts of Siberia 250 million years ago came from the lowermost mantle, up to 2900 kilometers below the Earth's surface. A small fraction of the rare and valuable metal platinum under l percent were discovered under the frozen wastes of Siberia may have come from the core [Hecht, 1995]. Two studies support it: (1). from the US and Russia report, the ratio of helium-3 to helium-4 in Siberian rocks is up to 12.7 times the atmospheric value. Primordial helium-3 leaked away from the surface of the young Earth but was retained in the lower mantle. High helium-3 levels had been found earlier in hot-spot lavas, indicating the lava came from the lower mantle [Basu *et. al.*, 1995]. (2). unusually high levels of osmium-187 have been found in sulphide rocks in the deposits. The extra osmium probably came from the decay of radioactive rhenium-187, which is thought to exist in high concentrations in the metallic core [Walker *et. al.*, 1995]. Thereby some materials are found in the deposits come all the way from the core. On the basis of some of the metal platinum in Siberia may have come all the way from the core of the Earth, the idea of D″ layer, which is considered to be virtually isolated the core from the rocky mantle and to sustain the chemical and the thermal equilibriums between the mantle and the core, may be challenged.

Knittle and Jeanloz (1991) suggest that a significant amount of the energy driving mantle convection is generated in the core. Checking the temperature of Earth interior, the hottest point is the center of Earth about 7000°C [Kubala & Rao, 1996], and in the inner-core boundary over 6000°C [Condie, 1997], and in the CMB about 4180 ±150°K [Fiquet *et al*., 2010], the abundant heat flow must from fluid core leaks out into mantle. In the higher resolution models, some of the heterogeneities extend upward from the CMB into the mantle in a manner suggestive of rising plume structure [Young & Lay, 1987]. Thermal plumes are tubes of hot rock rising from Earth's core, and carry more heat away [Hand, 2015], On this basis, a great quantity of magma heated by the extreme temperatures in the core solidifies into rock and produces the heat of solidification at the CMB. A few quantity of magma absorbing this heat does not solidify, but mixes with masses of rock as honeycombed blobs of rock and brings some materials, including magma, osmium-187, ^{3}He and a little metal as platinum, rising upward at approximately an inch a year through the mantle to pour out at cracks in the mid-ocean ridge to form new ocean floor or in the continent to form great rifts, to disperse the internal heat on the Earth’s surface that works as a secular cooling of the Earth. Approximately 80 % of the hot spots at the Earth's surface are manifestations of plumes rooted in the deepest part of the Earth. The outflow of heat is the dynamic source of continental drift.

Nevertheless, due to geological processes, the downward migrating masses of cold lithosphere plate in subduction zone of the crust may be driven through convection falling subduction slab all the way through the warmer surrounding mantle to the CMB. The downward masses of slab in the cold regions of the low mantle produce depressions of the CMB into the core, and both the cold region in the mantle and a depression of the CMB produce down welling flow in the core [Bloxham & Jackson, 1990].

The depressed regions of the topography on the CMB are dynamically supported by down welling of cool mantle materials [Gudmundsson *et al*., 1986; Lay, 1989], and then through CMB into liquid core that are

probably determined by processes in the core [Bloxham & Jackson, 1990]. In the outer core materials absorb the abundant heat flow, and forms an upward convection thermal plume again. Obviously the relief of CMB is dynamically supported and provides coupling materials between solid mantle and fluid core.

In this way, the materials of lower mantle and outer core mixing with each other, and the density distribution between both should be continuity in order to solve some problems in the geophysics. The main composition of outer core should be considered as the same ingredients of molten rock and/or mineral silicates, which are chemically consistent with the same ingredients of lowermost mantle.

The energy source and buoyancy source in the core are still not well understood, but we attempt to explain this phenomenon from the perspective of convection cell. The downward masses of slab absorb the heat of fusion, diminishing the heat energy at the CMB, and melting in the core where viscosity is so high that the large quantity of molten rock may not diffuse but still remain a whole. So, the components of molten rock are seldom involved in the chemical reactions.

According to mechanics, although the velocity of downward migrating flow is low, the mass of the slab column from the crust to the CMB is so large that its downward momentum has a great quantity. In the liquid outer core, there is no rigid body having enough mass to counteract the downward momentum, so the molten rock sinks all the way into the lowermost fluid core. The great downward momentum is counteracted merely by the solid inner core, which Jeanloz and Wenk (1988) have obtained a possible evidence of low-degree convention like it in the mantle in the inner core from an enigmatic observation.

Seismological studies indicate that the inner core of Earth is anisotropic for *P* waves, and has low *S* wave velocity, and high seismic attenuation. The presence of a volume fraction of 3 to 10% liquid in the form of oblate spheroidal inclusions aligned in the equatorial plane between iron crystals is sufficient to explain the seismic phenomena. The liquid could arise from the presence a "mushy zone" of dendrites or a mixture of elements other than iron that exist in liquid form under inner-core conditions [Singh *et al.*, 2000].

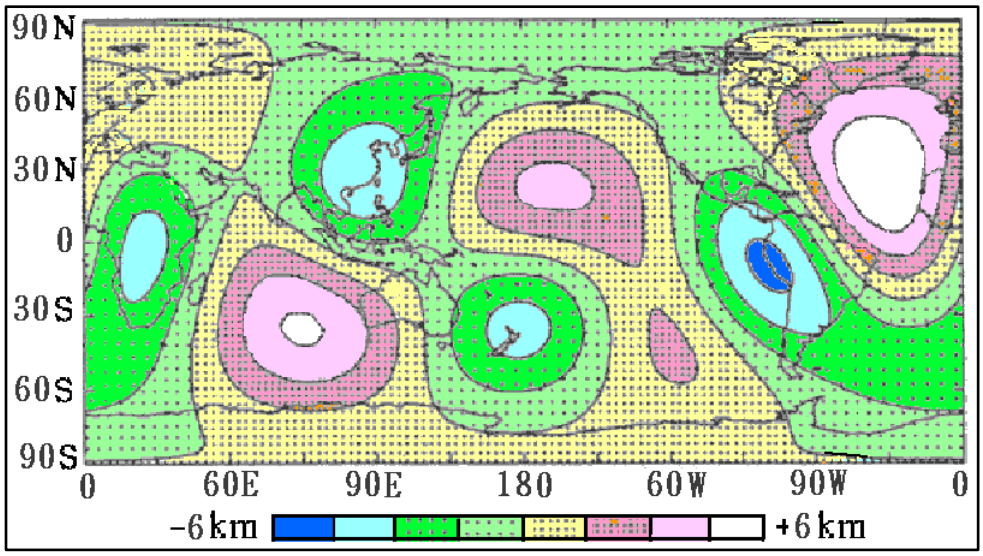

Fig. 1. Topography CMB obtained by inversion of the combined PcP and PKP_{BC} Data set. (Morelli and Dziewonski 1987).

Bergman (2003) and Shimizu *et al*. (2005) suggest that a thin mushy layer develops underneath the inner core boundary while the materials of outer core solidify onto the inner core. So, the inner core should be not a rigid spheroid.

The inner core rotation and high-quality teleseismic waveform doublets make the precise mapping of the topography of the inner-core boundary up to about 3.7 to 5.2 km. Dynamic models include a bumpy ICB rotating with the inner core itself or a transient slurry boundary containing a mixture of molten materials and solidified patches of iron crystals, which is rapidly modified by the turbulence at the base of the convecting outer core [Song & Dai, 2008].

At the ICB, the momentum from the downward molten rock is transmitted through the inner core, the Earth's center, and probably on to the opposite side of the CMB. This phenomenon can be inspected by the three-dimension topographic map of CMB in the Earth (Figure 1) [Morelli & Dziewonski, 1987]. All these it is magma that sinks toward ICB, and its kinetic energy becomes the pressure and spreads into the earth's inner core, and pushes and shoves the relative opposite side of the ICB, even to form the unsmooth CMB. From the diagram, the CMB is concaving in New Zealand, but protruding in the North Atlantic Ocean, and concaving under the west coast of South America, else protruding in region of Western Australia and near the Indian Ocean, and concaving under South Africa, also protruding in North Pacific Ocean too.

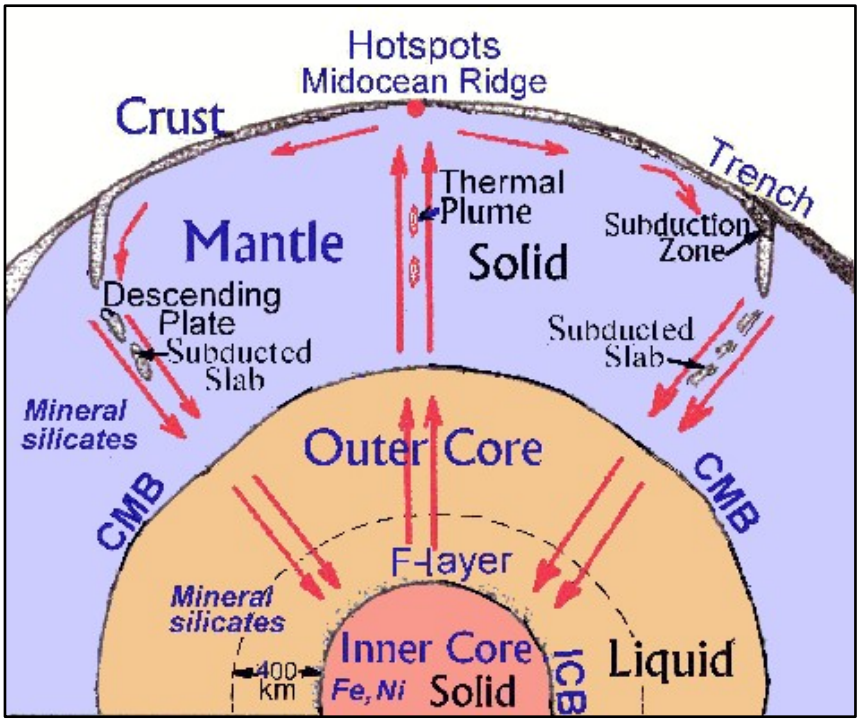

Fig. 2. A schematic diagram of the great convection cell: the thermal plume migrates up to the crust and subducted plate down to the F-layer of outer core and causes a relief of CMB topography over 10 km.

There is a significant suggestion that the same materials, dominantly silicates, of the rocky mantle and the liquid outer core change states with each other at the CMB to produce the relief of CMB topography over 10 km. A reasonable way may be figured out that the migrating rock or molten rock of plate sinks downward and magma or thermal plume rises upward in the great convection cell spanning the crust through the F-layer of outer core. A schematic diagram of the scenario is shown in Figure 2.

3.4. The arguments at the inner core boundary

The seismic structure of Earth's inner core is highly complex, displaying strong anisotropy and further regional variations. However, few seismic waves are sensitive to the inner core and fundamental questions regarding the origin of the observed seismic features remain unanswered [Waszek & Deuss, 2015a]. It is well accepted that the inner core solidifies from the outer core, but the details of this process are still largely unclear [Pejić & Tkalčić, 2016].

Seismologists have yet to answer some of the most fundamental questions concerning the core, one is the nature of the low-velocity gradient region at the lowermost outer core. A large number of seismological studies have suggested that the region just above the inner core boundary (ICB) is distinct from the rest of the outer core. The layer about 400 km above the ICB was originally termed the F-layer and was characterized by a strong low velocity zone [Jeffreys, 1939]. After the research of velocity and amplitude in the core, scientists infer the high separated solutions of the F-layer is around the ICB [Bolt 1972; Qamar 1973]. Most observations indicate that the F-layer is global and surrounds the entire inner core [Cormier, 2009; Souriau & Poupinet, 1991; Zou *et al.*, 2008; Cormier *et al.*, 2011].

From ray theory, an evidence of reduced seismic wave velocity gradient to near zero in F-layer of outer core has been interpreted [Rial & Cormier, 1980; Cormier, 1981]. Later Earth models, constructed with more accurate travel time data, instead defined this as a region of increased velocity. Among velocity models at the base of the outer core reported by different studies [e.g., Qamar, 1973; Dziewonski & Anderson, 1981; Choy & Cormier, 1983; Souriau & Poupinet, 1991; Song & Helmberger, 1995; Kennett *et al.*, 1995; Yu *et al.*, 2005], the main difference is the structure of the velocity and its gradient at the bottom 400 km of the outer core. According to the Earth's models, such as: AK135 [Kennett *et al.*, 1995], PREM2 [Song & Helmberger, 1995], and Jeffreys-Bullen model [Jeffreys, 1939; Bullen & bolt, 1986] denote a low-velocity gradient region at the lowermost outer core. In PREM [Dziewonski & Anderson, 1981], the velocity increases with a nearly constant gradient around 0.6×10^{-3} s^{-1}. In PREM2 and AK135, the velocity gradient decreases from about 0.6×10^{-3} s^{-1} at 400 km above the ICB to nearly zero at the ICB, and the velocity profile with depth is more flat than that in PREM (Figure 3). Therefore, 400 km above the ICB is chosen as the minimum 'pinning depth', at which the models are evaluated and constrained to agree with PREM in value and gradient.

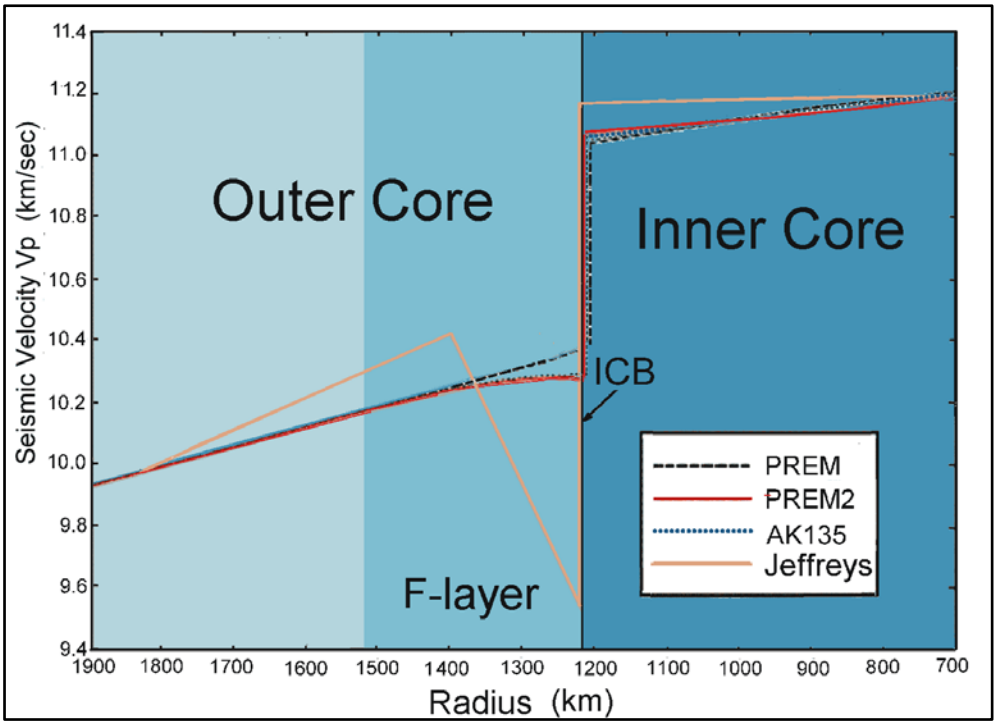

Fig. 3. A comparison of seismic P velocity (Vp) and **S** velocity (Vs) distributions is given among the Earth models of Jeffreys-Bullen, Ak135, PREM2 and PREM. The comparison indicates that the velocity curves closely agree generally, but the main exceptions are that the low-velocity zone F-layer in the Vp curve.

While the seismic wave enters F-layer, a sharp velocity discontinuity at ICB, the velocity jumped 0.78

km/sec, and a low velocity gradient at the base of the fluid core that indicates slightly different properties of the components. The most robust pointer to a viscosity at the bottom of the outer core may be still its reduced P velocity gradient, which is difficult to explain without appealing to the existence of a chemical boundary layer [Kennett *et al*., 1995; Song & Helmberger, 1995]. These models imply that near the base of the outer core density increases too quickly to be explained solely by compression, and some sort of change in chemistry and phase may occur.

Experiments [Sumita & Olson, 1999, 2002] and numerical simulations [Aubert *et al*., 2008] have shown that temperature anomalies generated by strongly heterogeneous CMB heat flux can be transmitted from the CMB to the ICB by outer core convection. As the Earth cooled and dissipated its internal heat toward the surface of the Earth through mantle convection, the geographical coincidence of the ICB and CMB anomalies may suggest strong thermal coupling of the mantle and the core that means there is a convection cell across CMB. The F-layer should have some functions instead that of the well-known D" layer, such as the thermal and chemical equilibrium.

The regional differences in *PKIKP-PKiKP* travel times and *PKiKP*/*PcP* amplitude ratio data may originate from the F layer instead. Bolt and Qamar (1970) first proposed the amplitude ratio (*PKiKP/PcP*) technique and estimated a maximum density jump of 1.8 g/cm^3 at the ICB. Bolt (1972) clearly observed both low angle and steep incident reflections *PKiKP* of about one second period at the ICB. The mean amplitude ratio *PKiKP/PcP* suggests a density jump $\Delta\rho$ of 1.4 g/cm^3 here. Souriau and Souriau (1989) used the amplitude ratio *PKiKP/PcP* at short distances to constrain the density jump at the inner core boundary to be in the range of 1.35～1.66 g/cm^3 based on array data. Shearer & Masters (1990) used "non-observations" of *PKiKP* on the observed amplitude of this phase, leading to upper bounds $\Delta\rho$=1.8 g/cm^3 at inner core boundary on the corresponding *PKiKP/PcP* amplitude ratios. Studies used *PKiKP* to calculate the density jump $\Delta\rho$ across the inner core boundary, and this has remained a topic of debate to the present day [Waszek & Deuss, 2015b]. At the ICB, a density jump of 0.68 g/cm^3 in the PREM is too small to compare with the previous data.

As stated previously, the difference in density between the outer core and the inner core must be great. Jeanloz and Ahrens (1980) completed shock-wave experiments, in which it was found that the density of FeO is 10.14 g/cm^3 when reduced to core temperature and 250 GPA pressure, and under the same conditions the density of Fe is12.62 g/cm^3 [McQueen *et al.*, 1970] when FeO becomes Fe. The difference between both is 2.48 g/cm^3, a figure higher than all of the other evaluated values.

From this information other than the PREM, the density jump between the lighter liquid outer core and the solid inner core seems to be too large to represent a simple volume change on condensing as the same major components change from a liquid state Fe into a solid state Fe. The composition of the outer core is not likely to be the same as the inner core, since a liquid in equilibrium with a solid phase in a multi-component system does not have the same composition as the solid [Hall & Murthy, 1972]. We infer that the major component of outer core is mineral silicates, but iron in the solid inner core.

On the basis of the free oscillation periods, Derr (1969) has inferred an earth model DI-11 by least-squares inversion with an average shear velocity of 2.18 km/sec in the inner core and a jump in density of 2.0 g/cm^3 at its boundary that satisfies the known mass and moment of inertia. We use the largest density jump of Derr's suggestion 2.0 g/cm^3 at the ICB to research the new earth model in this paper.

3.5 Examining the chemical composition of the core

In order to confirm a favorable constitution of the Earth, the chemical composition of the core must be further investigated. The composition of the Earth's core is one of the most important and elusive problems in geophysics. There is no perfect explanation of the chemical equilibrium between the core and the mantle, and the inner core is not in thermodynamic equilibrium with the outer core [Jeanloz, 1990].

The physical and chemical properties of the lower mantle are poorly known, and the understanding of the coupling mechanisms between the mantle and the core is poor on all timescales. But the CMB sets boundary conditions for processes occurring within the core that is a well-known fact. The topography and the lateral temperature variations in the lowermost mantle may have an indistinguishable effect on the magnetic field [Bloxham & Gubbins, 1987]. Secular variations with periods shorter than a million years, but longer than several years, almost certainly originate from processes operating in the outer core; unfortunately, there is not yet consensus as to what those processes are [Mcfadden & Merrill, 1995].

In three-dimensional maps, topographic models represent an instantaneous, low-resolution image of a convicting system. Detailed interpretation knowledge of mineral and rock properties that are, as yet, poorly known is required. A complex set of constraints on the possible modes of convection in the Earth's interior that have not yet been worked out; this will require numerical modeling of convection in three dimensions. Thus the interpretation of the geographical information from seismology in terms of geodynamical processes is a matter of considerable complexity. The topography on the CMB can be sustained only by dynamic processes, and these processes must be crucially understood [Woodhouse & Dziewonski, 1989].

The fine structure of the CMB is not well known, but it contains information important to the geodynamic processes in the mantle or in the magnetic field generated in the outer core [Dziewonski & Woodhouse, 1987]. Approaching the Problem of the CMB, Creager and Jordan (1986) studied travel-time anomalies of *PKiKP* and PKP_{AB} and corrected for the mantle structure onto a region in the vicinity of the CMB. They consider some hypotheses with regard to the source of anomalies that are the perturbations in the CMB topography. Based on the great convection cell a relief of the core in excess of 10 km provided by the three-dimensional maps may be accepted.

As stated previously, the main components of the outer core are similar to the main components of the lower mantle, i.e. mineral silicates. Based on mineralogy, the main mineral of the mantle is pyrolite, a compound of silicates, and the main components of the outer core are also pyrolite but only in a liquid state. Under the same conditions, the higher the temperature under which common minerals are produced, the lower the polymerization is and vice versa. The closer the crystal minerals of the mantle under the temperature and pressure are to the core, the more the polymerization losses of crystalline mineral. Then the bonding forces of

mineral compound are destroyed and the crystallization gradually diminishes.

For example, olivine, an important rock of the Earth, under room temperature and pressure is a complex crystal tectosilicate. Quartz is a mineral of olivine. After heating, quartz, the four oxygen of the silicon oxygen tetrahedron and four different structures of the silicon oxygen tetrahedron, are gradually reduced to phyllosilicates, inosilicates and cyclosilicates, respectively. When the temperature raises considerably high, the four oxygen of silicon oxygen tetrahedron become an elemental unit of silicates known as sorosilicates. When the temperature approaches the melting point, the sorosilicates become the nesosilicates, which are the crystal tetrahedron of silica mineral, a basic structural unit of minerals.

At reaching the CMB, olivine reduces phyllosilicates, inosilicates, cyclosilicates, sorosilicates and nesosilicates respectively, when the temperature rises considerably high (4180 ±150°K [Fiquet *et al*., 2010]) and reaches the melting point of solid rock, some of the rock melts in the core and liquefies into the molten rock. In the F-layer of the deeper core, the high temperature more than 6000°C [Condie, 1997], polymerization may cease completely, and mostly bonding power of ions loses, only the electronic bonding force exists. All the ions and molecules may become unbounded. Therefore, the molten rock or magma becomes a mixture of oxides such as FeO, MgO, NiO, SiO_2, Fe_2O_3, Al_2O_3, Cr_2O_3, etc., and metals, such as Fe, Ni, Mn, etc.

According to temperature profile of Earth's interior, the center of Earth is made up of high temperature material, which is the hottest point, estimated to be 7000°C [Kubala *et al*., 1996] that is hotter than the surface of the Sun. In F-layer, the chemical components maybe reduce the viscosity, the full fluid oxides and metals are able to flow, and diffuse, float or sink more freely according to its specific gravity. Estimation of Fe melting temperature at ICB pressure based on static compression data spans the range 6230 ± 500°K [Anzellini *et al.,* 2013]. The F-layer above the ICB, in which Fe likes snowflake falling in the inner core [Gubbins *et al.*, 2008].

There are a large amount of iron oxides (FeO, Fe_2O_3) in the mantle, and the deeper the mantle, the higher the proportion of iron oxides is. An iron oxide which has metal-like density and electrical properties at high pressure and temperature exists in the Earth's core maybe a compromise between extreme views of the metallic phase and inconformity with the high cosmic abundance of oxygen [Altshuler & Sharipdzhanov, 1971]. From this information, the outer core is rich in iron oxides are proposed.

In view of the topography, the downward migrating magma rich in iron oxides is affected by diffusion, obstruction of the inner core, tangentially geostrophic flow and toroidal flow, so the fluid flows westward, which may causes the geomagnetic secular variation. Under low viscosity, the oxides and metals can vertically and horizontally flow easily, thus allowing mutual oxidation-reduction reactions to take place in the F-layer. The active light metals take oxygen from heavy metal oxides and are further oxidized into light metal oxides, and the heavy metal oxides are reduced to heavy metals and falling precipitation in the inner core. For example:

$$Ca + FeO \longrightarrow CaO + Fe\downarrow$$

$$3Mg + Fe_2O_3 \longrightarrow 3MgO + 2Fe\downarrow$$

$$2Al + Fe_2O_3 \longrightarrow Al_2O_3 + 2Fe\downarrow$$

$$2Cr + 3FeO \longrightarrow Cr_2O_3 + 3Fe\downarrow$$

$$Mn + NiO \longrightarrow MnO + Ni\downarrow$$

CaO, MgO, Al_2O_3, Cr_2O_3 and MnO float in the F-layer, and Fe_2O_3, FeO and NiO become iron and nickel, which sink down to be the main component of the inner core. These oxidation-reduction reactions are exothermic processes that produce a great amount of heat. The reduced iron alloys with certain amounts of nickel settle down at the ICB. By far the most provocative mechanism, the F-layer should be maintained through the interaction of separated melting and solidifying regions distributed over the ICB [Alboussière *et al.*, 2010]. In the F-layer, magma diffuses and absorbs a great amount of heat to rise to the CMB and condenses into solid rock as the beginning of the process of a large convection cell starts anew. The great amount of heats, produced from radioactive elements generated nuclear energy, chemical reaction heat in the F-layer and nuclear fission heat near the center of the Earth, become the power sources for the geo-dynamo of great convection cell. (Figure 4). Therefore, the Earth's geomagnetic secular variations and the geodynamical processes operates from the F-layer of outer core.

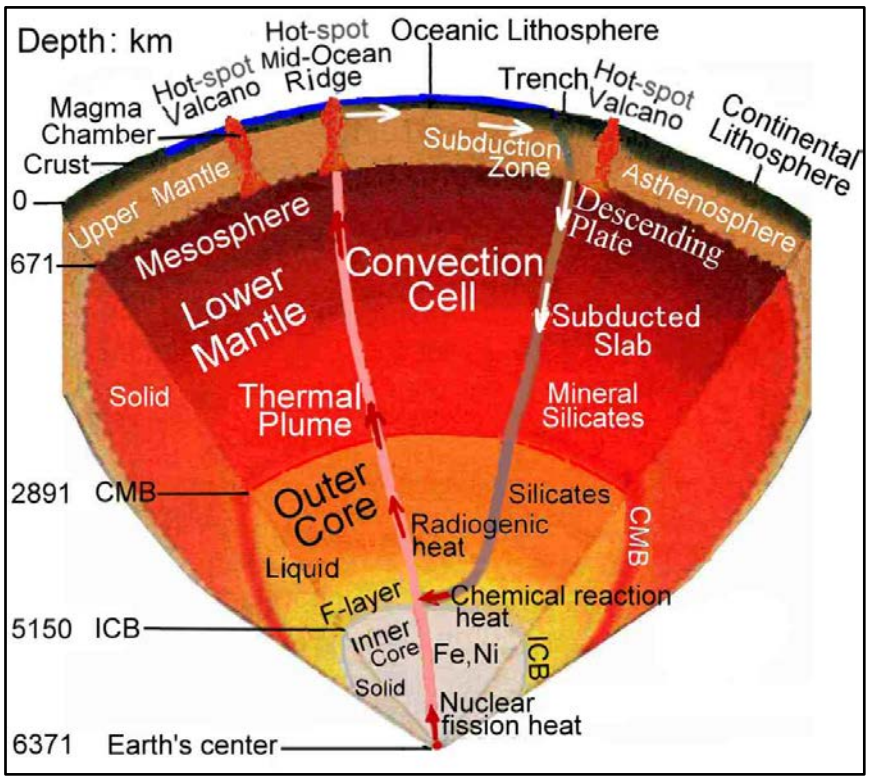

Fig. 4. A schematic diagram of a great convection cell and heat flow, and the composition of Earth's interior.

4. Digital evaluation of the data in the new earth model

In order to calculate the data of the Earth, the density distribution follows the divisions of the PREM divided into 94 levels, including 82 thin shells. The thickness of each shell is not greater than 100 km and so small compared with the Earth's radius of 6371 km that the density is regarded as linear variation within it. Then, a simplified method is applied to calculate the information of the Earth in order to simplify the calculating work [Ho, 1993].

The formula for the mass M of a uniform sphere can be derived through $M = (4/3)\pi\rho R^3$. The mass ΔM of each shell in the Earth's interior can be calculated through

$$\Delta M = (4/3)\pi\rho_t R_t^3 - (4/3)\pi\rho_b R_b^3 \quad (1)$$

Where ρ_t, ρ_b are the densities at the top and the bottom, respectively, of one shell, and R_t, R_b are the radii of the top and the bottom in a shell. Because the difference between R_t and R_b is so small and the density

is regarded as linear variation in the shell, the mean value $\bar{\rho}$ of both ρ_t and ρ_b is substituted for ρ_t and ρ_b in order to simplify the calculation. Then equation (1) becomes

$$\Delta M = (4/3)\pi\bar{\rho}(R_t^3 - R_b^3) \quad (2)$$

The moment of inertia of a sphere can be derived through $I = CMR^2$. Where C is the coefficient of the moment of inertia, which is 2/5 in a uniform sphere. The moment of inertia ΔI of each shell in the Earth's interior can be calculated through

$$\Delta I = (8/15)\pi\bar{\rho}(R_t^5 - R_b^5) \quad (3)$$

From fluid mechanics, in a region of uniform composition, which is in a state of hydrostatic stress, the gradient of hydrostatic pressure is expressed by

$$dP/dR = -g\rho \quad (4)$$

Where P, R are the pressure and the radius, respectively, at the region; ρ is the density at that depth; g is the acceleration due to gravity at the same depth.

If the effect of the Earth's rotation is negligible, the potential theory shows that g is resulted only from the attraction of the mass M within the sphere of radius R through

$$g = GM/R^2 \quad (5)$$

Where G is the gravitational constant 6.6726×10^{-11} $m^3/kg.s^2$.

Equation (5) substitutes into equation (4) and integrate it. In order to simplify the calculation, ρ and M are substituted by $\bar{\rho}$ and $\bar{m}$, which are considered the constants in the thin shell and irrelative to the P and R. The result becomes

$$\Delta P = (1/R_b - 1/R_t)G\bar{m}\bar{\rho} \quad (6)$$

Where ΔP is the difference in pressure between the top and the bottom in a layer of the Earth, and $\bar{m}$ is the mass of a sphere as the mean value of the masses of the sphere within the top radius R_t and the bottom radius R_b, respectively, of a shell.

Equation (6) cannot be applied to the center of the Earth where is a discontinuous point. To integrate the portion of the center, the other form is applied as

$$\Delta P_c = (2/3)\pi G\bar{\rho}^2 R_c^2 \quad (7)$$

Where ΔP_c is the difference in pressure between the radius Rc and the center of the Earth at the center portion.

The acceleration due to gravity g of each layer can be derived from equation (5). According to the observation data, the moment of inertia about the polar axis of the earth is $0.3309 M_e R_e^2$ and about an equatorial axis is $0.3298 M_e R_e^2$ [Garland 1979]. The earth is regarded as a sphere, of which the moment of inertia is determined to be 80286.4×10^{40} $g.cm^2$ by taking the mean value of both figures, where Me is the earth's mass of 5974.2×10^{24} g and Re is the equatorial radius of 6378.14 km.

In order to examine the accuracy of applied equations, we apply the density distribution of the PREM to calculate the Earth's mass, moment of inertia, pressure and acceleration due to gravity in Table 2 (http://newidea.org.tw/pdf/S60.pdf). The calculated values of the earth's data from the density distribution of

the Preliminary Reference Earth Mode as compared with the values of the current data and the PREM are listed in compared with that of the current data and the PREM are listed in Table 3.

Table 3. The calculated values of the simple method from the density distribution of the PREM as compared with the data of the PREM and the current earth.

Data of the Earth	Mass	Moment of inertia	Pressure at CMB	Pressure at Earth center	Gravity at CMB	Gravity at Earth surface
Unit	10^{24} g	10^{40}g.cm^2	kbar	kbar	cm/sec^2	cm/sec^2
PREM & Current	5972.200	80286.400	1357.509	3638.524	1068.230	981.560
Calculated values	5973.289	80205.664	1358.335	3655.973	1068.680	981.959
Difference %	-0.0152	-0.1006	+0.0608	+0.4796	+0.0421	+0.0406

From Table 3 the deviations of the calculated Earth's values from the data of the PREM and the current Earth are nearly within 0.1%, except the pressure at the Earth center. It indicates that the calculated values are very close to the current data and the simplified method is acceptable and useful; however, the calculated pressure of 3655.973 kbar at the Earth's center is higher than the data of the PREM of 3638.524 kbar by 0.4796 %, about 8 times of deviation at the CMB.

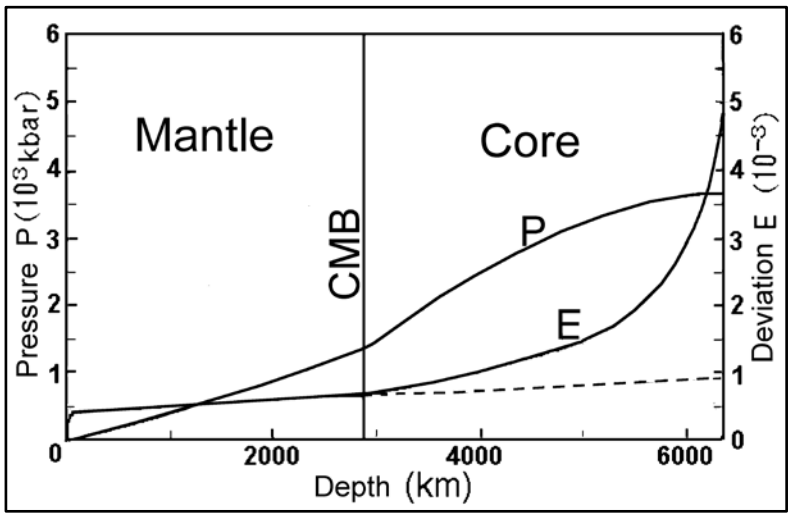

Fig. 5. The pressure P of the PREM and the deviation E of the calculated pressure of simplified method from the value of P.

We compare all the calculated pressures of the simplified method with that of the PREM by the curve of deviation E in Table 4 (http://newidea.org.tw/pdf/S61.pdf) and show the pressure P of the PREM in Figure 5. According to the Figure 5, the deviations E of Pressure curve from the crust to the CMB is showed nearly as a straight line, indicating that the calculated pressures have the systematic errors in view of the error theory. But from the CMB to the Earth's center, the slope of curve E sharply increases above the dashed line, which is the straight line extended from the CMB. It indicates that there is a considerable discrepancy within the core. We may suppose that the structure of the core in the PREM, which greatly affects its core pressure, is something wrong.

In order to investigate the structure of the Earth, particularly the core, four curves of density distribution are proposed to match the known conditions. From the crust to the CMB the curves of density distribution are adopted as the same of the PREM, and from the CMB to the ICB four plotted different curves are assumed. Due to a small jump of P-wave velocity at the boundary of F-layer in the outer core, the slope of density curve is nearly as steep as the PREM. There is a discontinuity at the ICB, so that a density jump of Derr's (1969)

suggestion (2.0 g/cm^3) is used. In the inner core, the same slope of density curve of the PREM is used. The four density curves of the assumed Earth model compared with the PREM are shown in Figure 6.

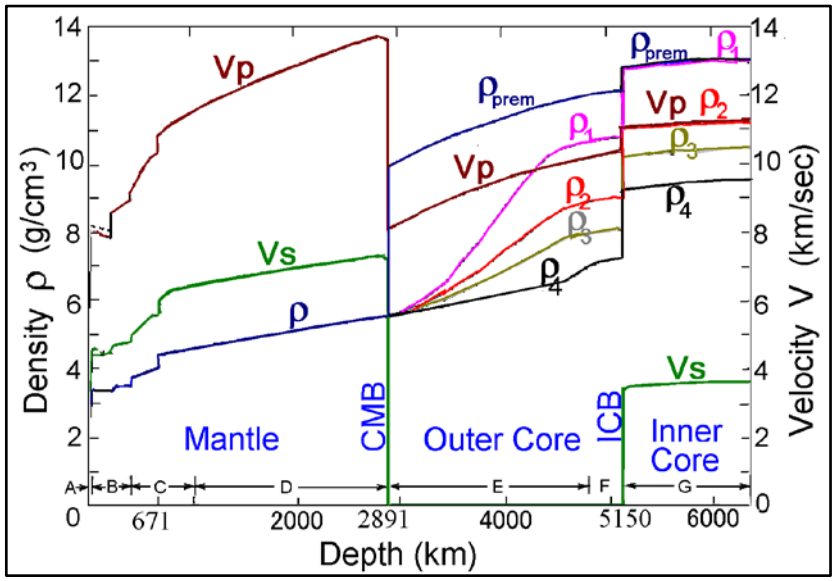

Fig. 6. These densities ρ of the new Earth models 1, 2, 3 and 4 are compared with the PREM's.

The mass and the moment of inertia of four new Earth models can be determined, and compare with the current measured data (1990s) of the Earth's mass of 5974.2×10^{24} g and moment of inertia of 80286.4×10^{40} g.cm^2, then the differences will be found to be very large as Table 5 is shown. The differences are the insufficiencies of the mass and the moment of inertia of the four new Earth models.

Table 5. The insufficiencies of the mass and the moment of inertia in the four new earth models.

Earth model	Unit	Observed value	New model 1	New model 2	New model 3	New model 4
Mass	10^{24} g	5974.200	5409.024	5268.126	5204.761	5121.820
Insufficiency	10^{24} g		565.176	706.074	769.439	852.380
Moment of inertia	10^{40} g.cm^2	80286.400	77007.472	76571.028	76378.768	76126.841
Insufficiency	10^{40} g.cm^2		3278.928	3715.372	3907.632	4159.559

The insufficiencies of the Earth's mass and moment of inertia, called the missing mass and moment of inertia, both are relative to the gravity that belong to the dark matter in astrophysics. It can only be obtained by comparing the observed data of the Earth, but cannot be detected directly and answered clearly through the ordinary Earth sciences. In order to solve the problems of the insufficiencies, a new study of the Earth is attempted by utilizing the contemporary physics. If we can successfully explain that the insufficiencies exist in a suitable condition, a new Earth model will be established.

There are two types of dark matter: hot dark matter (HDM) and cold dark matter (CDM). Hot dark matter exists as such in a kind of photon or neutrino which has zero mass and moves at or approaching the speed of light. Cold dark matter exists at a lower energy and particle type. Due to the gravity of the particles, CDM moves at a low speed and collects together like normal matter. According to the observation data of background radiation in the universe, some physicists have recently proposed that perhaps cold dark matter

explains the cosmic-structure. Blumenthal *et al.* (1984) argued that the CDM model for the formation and distribution of galaxies in the universe is successful and the expansion of the universe is dominated by the CDM. After reporting the South Pole experiment, Lubin *et al.* (1991) showed that according to a recent anisotropy experiment in which a Byesian analysis was used to constrain the amplitude of the perturbation spectrum, they showed that adiabatic HDM models were convincingly ruled out and CDM models had anisotropies near their derived limits. Based on the result of their experiment, they announced the South Pole experiment was particularly well suited to the CDM-type model, among others.

Proceeding with the assumption, the missing mass and moment of inertia of the Earth are those of the CDM, which may constitute a normal planet. In order to find some solution in this article, the dark matter is compared to Mars. The average radius of Mars is 3397 km, and the mass 642.40×10^{24} g. Kaula *et al.* (1989) studied the moment of inertia of Mars and got the maximum allowable mean value is 0.3650 MR^2, i.e. 2689.8×10^{40} g.cm^2. The insufficient data of 4 new Earth models roughly approach to the Mars', So, the dark matter is considered as a planet, called a dark planet, of which the form is similar to Mars and its characteristics are based on the inner planets of the solar system. In order to cut a figure of the dark planet, it is considered as a sphere, whose radius and density can be calculated from the insufficiencies of the Earth's mass and moment of inertia through the simplified method. The data of the dark planet can be calculated as following.

Considering the density of rock on the surface of the Earth and the Moon, the surface density 2.70 g/cm^3 of the dark planet is proposed. Under the condition that the density of a layer is proportional to its depth, a trial value of density at the center of the dark planet is selected, and applying the equations (2) and (3) to calculate the mass and the moment of inertia of each shell, the total mass and moment of inertia of it should be gotten. Because the radius and the center density of the dark planet are the hypothetical values, but the total mass and moment of inertia are necessary to correspond to the insufficiencies of the Earth's; therefore, it is necessary to use a trial-and-error approach to determine the proper radius and the center density.

Since the Earth's orbit around the Sun may be affected by the gravity of the dark planet, but no abnormal effect on the Earth has been observed. An assumption is suggested that the gravity centers of the Earth and the dark planet coincide with each other at the same point. It is inferred from the phenomenon in which the same side of the Moon always faces the Earth that means the Earth and the dark planet may rotate synchronously.

Assuming that the gravity centers of the Earth and the dark planet coincide at a single point and both rotate synchronously, the total values of mass and moment of inertia may be obtained from the sum of them. Based on mechanics, the gravity at each shell inside the Earth is affected by the mass of the Earth and the dark planet within its radius. The pressure difference $\Delta P'$ between the top and the bottom of a shell within the Earth is calculated through

$$\Delta P' = (1/R_b - 1/R_t)G\overline{M}'\overline{\rho} \qquad (8)$$

Where $\overline{M}'$ is the mean value of the total mass of the Earth and the dark planet within the radius R_t and R_b.

Equation (8) cannot be applied to the Earth's center. The average density $\overline{\rho}'$ of the central portion combined with the Earth and the dark planet within the radius Rc can be calculated through

$$\overline{\rho}' = (Mc + Md) / [(4/3)\pi R_c^3] \quad (9)$$

Where Mc and Md are the masses of central portion in the Earth and in the dark planet, respectively.

The difference of pressure $\Delta P_c'$ between the top and the center of the central portion in the Earth can be obtained through

$$\Delta P_c' = (2/3)\pi G \overline{\rho}\,\overline{\rho}' R_c^2 \quad (10)$$

Based on the characteristics of the inner planets of the solar system except Mercury, the bigger the radius of a planet, the higher the average density is. So, the radius and the average density of a suitable dark planet must be compatible with the characteristics of inner planet in solar system. The data of the four new Earth models and each dark planet are compared with the data of the current Earth and the PREM in the Table 6.

Table 6. The calculated data of the new four earth models compared with the data of the current earth and the PREM.

Kind of Earth's model	The Earth planet							The dark planet					Suitability
	Radius	Average density	Mass	Moment of inertia	Center density	Center pressure	Moment of inertia coefficient	Radius	Average density	Mass	Moment of inertia	Moment of inertia coefficient	
Unit	km	g/cm^3	10^{24} g	10^{40} g·cm^2	g/cm^3	kbar	C	km	g/cm^3	10^{24}g	10^{40} g·cm^2	C	
PREM	6371	5.5150	5974.200	80286.400	13.08848	3638.524	0.3309						
Model 1	6371	4.9935	5409.024	77007.472	13.08848	3283.754	0.3508	3808.414	2.4427	565.176	3278.928	0.4000	no
Model 2	6371	4.8635	5268.126	76571.028	11.29785	3039.584	0.3581	3732.304	3.2421	706.074	3715.372	0.3777	no
Model 3	6371	4.8050	5204.761	76378.768	10.46002	2934.587	0.3615	3717.755	3.5747	769.439	3907.632	0.3674	no
Model 4	6371	4.7284	5121.820	76126.841	9.49821	2805.297	0.3662	3700.375	4.0161	852.380	4159.559	0.3564	good

The average radius of Mars is 3397 km, the mass 642.40×10^{24} g, and the average density 3.912 g/cm^3. Both values of the radius and the average density of the dark planet in the new Earth model 4 are bigger than those of Mars, therefore, this model is found to be the more suitable one.

The precise data of the Earth and the dark planet are calculated from the density distribution of the new Earth model 4, the Earth planet is listed in Tables 7 (http://newidea.org.tw/PDF/S62.pdf), the dark planet is listed in Table 8 (http://newidea.org.tw/PDF/S63.pdf) and the global data of the new Earth model in Table 9 (http://newidea.org.tw/PDF/S64.pdf). The pressure P and the acceleration due to gravity g of the new Earth model compared with the PREM are shown in Figure 7. In this suitable model the slope of density curve from a depth about 400 km of the upper mantle through zones C, D and E to the upper boundary of F-layer is nearly a straight line, which means the density increase in proportion to its depth in accord with general physical phenomenon. So, the new Earth model 4 is acceptable as the proper new Earth model. We can find the pressure curve of the new Earth model is smoother than that of the PREM below the CMB. In the gravity curve of the new Earth model, there are two deflection points in the curve that the one is at 2670.625 km in depth at the

radius of the dark planet, and the other is at the ICB. The Earth has a mass of 5121.820×10^{24} g, a moment of inertia of 76126.841×10^{40} g.cm^2, an average density of 4.7284 g/cm^3. The Earth's center has a density of 9.49821 g/cm^3 and the pressure of 2805.297 kbar. The reduced values of the Earth's data from those of the current Earth are due to the existence of the dark planet. The dark planet has a radius of 3700.375 km, a moment of inertia of 4159.559×10^{40} g.cm^2, an average density of 4.0161 g/cm^3 and a mass of 852.380×10^{24} g about 1.33 times of Mars. The data of the new Earth model compared with those of the current Earth and the PREM are listed in Table 10.

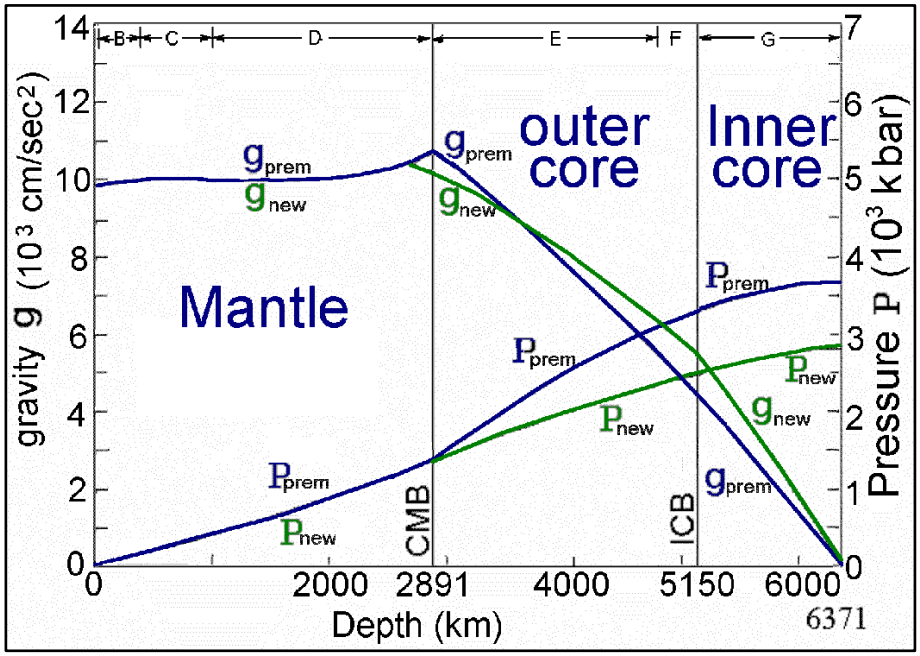

Fig. 7. Diagram of the gravity g and the pressure P of the new Earth model and the PREM

Table 10. The data of the new Earth model compared with the current Earth and the PREM.

Data of planet	Radius	Mass	Inertia of moment	Average density	Center density	Center pressure	Coef-ficient
Unit	km	10^{24} g	10^{40} g.cm^2	g/cm^3	g/cm^3	kbar	C
PREM and current earth	6371.000	5974.200	80286.400	5.515	13.08848	3638.524	0.3309
Earth planet	6371.000	5121.820	76126.841	4.7284	9.49821	2805.297	0.3662
Dark planet	3700.375	852.380	4159.559	4.0161	7.96097	1115.272	0.3564

The density of the Earth's center is 9.49821 g/cm^3, which is much lower than 13.08848 g/cm^3 of the PREM. Its pressure is 2805.297 kbar, which is also much lower than 3638.524 kbar of the PREM. The composition of the inner core is generally believed to be dominantly iron with a small amount of alloyed nickel. From the pressure-density Hugoniot data, the density of iron under 2805.297 kbar of pressure is about 12.7 g/cm^3 [Ahrens, 1980], which is much greater than that of the new Earth model by 25%. The inner core is not pure iron but contains a significant fraction of light components [Ringwood, 1984; Jephcoat & Olson, 1987], and that explains why the density of the inner core is so much smaller than the current value. Therefore, an inference that the composition of the inner core is dominantly iron, alloyed with a small amount of nickel and also combined with a significant amount of oxides is suggested.

5. Discussion and Result

Based on the new try, a study in a different view of the core, a great convection cell is developed, a circulation of magma and solid or molten rock migrating up to the crust and down across the CMB to the lowermost F-layer of outer core, causes the topography of the CMB, and from the core brings some matter as the metal platinum have come all the way to the surface of the Earth. This study introduces a new Earth model which should solve some inexplicable problems of the Earth science, such as the density jump, the core-mantle chemical equilibrium, the geomagnetic secular variation and the Chandler wobble. The anomalous properties of the CMB and the ICB should be apparently brightened after this study.

From the simplified method of evaluating the data of the new Earth model, compares with the current observed data of the Earth, there are 14.27 % of the mass and 5.18 % of the moment of inertia missing. From the conceptions of the String theory, a dark planet inside the Earth, whose mass and moment of inertia supply the missing portions of the current Earth, is virtuously developed. String theory has been pointed out by critics that the model has shortcomings and potential theoretical problems [Kaku, 1988]. Among those problems, the most fundamental one is that geometric formulation of the model has not been well understood yet. If the geometry underlying the String theory has been determined that may give us the key insight into the model and will allow us to make definite predictions with the String theory.

From10-dimensional space-time of the String theory develops a multiverse, which are three-cosmic framework of the Universes. After studying the existence of the dark planet in the Earth's interior, the three-cosmic framework of the Universes may be able to be confirmed. This result may be served as an indirect proof of the existence of the dark matter, which locates in the interior of the Earth but other space than ours. According to this framework there are triple Universes in the whole spaces, namely 1st Universe, 2nd Universe and 3ird Universe. The three-cosmic framework of U1, U2, and U3 have no relationship between any two Universes. In there no interacting force of nature exists, except gravitation force that is the characteristic of the dark matter. So, the dark planet, which is found through the gravity, may be in invisible space other than our Universe.

Scientists assume existence of "dark energy", which will cause the stars of the Universe expanding at an accelerating rate. But what dark energy is now the public knows nothing and unable to search. Since dark energy, by convention, does not count as "matter", from data gathered by the Planck spacecraft, this is 26.8/ (4.9 + 26.8) = 84.5 (%). We can only detect the whole Universe 15.5 % normal matter, but 84.5 % dark matter, which may be the star’s mass in other Universes than ours.

Cosmologists studying a map of the universe from data gathered by the Planck spacecraft, the map shows a stronger concentration in the south half of the sky and a 'cold spot' that cannot be explained by current understanding of physics. In 2005, Dr. Laura Mersini-Houghton, theoretical physicist at the University of North Carolina, and Professor Richard Holman, professor at Carnegie Mellon University, predicted that anomalies in radiation existed and the phenomenon can only have been caused by the pull of gravitational force from other Universes [Woit, 2013]. Because of containing the great quantity of stars 84.5 % in the other

Universes, its mass are pulling the stars of our Universe accelerating expansion by gravity. Scientists interpret it is the effect of dark energy to cause, in fact, there is only a great amounts of dark matter in our Universe, but no dark energy. The cold spot may be the first 'hard evidence' that other universes exist has been found by scientists.

It is hard to examine the existence of the dark planet directly; however, that can be recognized from Chandler wobble. Referring to the orientation of the rotation axis of the Earth in space in addition to both precession and nutation, there is a wobble on the instantaneous axis of rotation of the Earth itself. The wobble alters the position of a point on the Earth relative to the pole of rotation. Chandler (1891) pointed out that there are two different kinds of the wobble periods. One is a period of 12 months and the other is a period of 433 days, about 14 months. The former, called annual wobble, is obviously affected by the seasonal climate. The latter, called Chandler wobble, has not been solved the problem for more than one hundred years. The Chandler wobble is a small deviation that amounts to change of about 9 meters (30 ft.) at the point in the surface of the rotation axis of the Earth.

Gross (2000) found that two-thirds of the Chandler wobble was caused by fluctuating pressure on the seabed, which, in turn, is caused by changes in the circulation of the oceans caused by variations in temperature, salinity and wind. The remaining third is due to atmospheric fluctuations. The full explanation for the period also involves the fluid nature of the Earth's core and oceans. The wobble, in fact, produces a very small ocean tide with an amplitude of approximately 6 mm, called a "pole tide", which is the only tide not caused by an extraterrestrial body. While it has to be maintained by changes in the mass distribution or angular momentum of the Earth's outer core, atmosphere, oceans, or crust (from earthquakes), for a long time the actual source was unclear, since no available motions seemed to be coherent with what was driving the wobble.

Since that both the Earth and the dark planet spin synchronously around the same gravity center are postulated, but the rotation axes of both are impossible coinciding with each other. In other words, an angle between the two rotation axes produces the Chandler wobble as the precession and nutation due to the effects of the Sun and the Moon on non-parallel rotation axes with the Earth’s. Therefore, the effect of Chandler wobble may confirm the existence of a dark planet inside the Earth.

From this study, the hypothesis of the three-cosmic framework of the Universes maybe enable a new way to find out about the abundant dark matter and solve some problems in astrophysics, such as:

1. Cygnus X-1 is a hot super giant star orbited by an invisible compact object in a period of 5.6 days [Stokes & Michalsky, 1979]. The mass of the compact object can be estimated from the Doppler shifts in the spectrum of the visible super giant star. Its mass is about 9 times of the sun. This is considerably more than the maximum mass of a neutron star. Therefore, the compact object is not a neutron star or a white dwarf star. Since it has problems of optical confirmation, it is believed that the compact object may not be a black hole. If we consider the compact object of Cygnus X-1 as the dark matter in the other Universe than ours and its gravity affects Cygnus X-1, the problem may be solved.

2. Stars that evaporate from the Hyades cluster will remain within a few hundred parsecs (1 parsec＝3.26 light year) of the cluster only if they are dynamically bound to a much more massive entity containing the cluster. A local mass enhancement of at least (5-10)×10^5 solar masses, with a radius of about 100 pc, can trap stars with an origin related to that of the Hyades cluster and explains the excess of stars with velocities near the Hyades velocity that constitutes the Hyades supercluster. Part of this mass enhancement can be in visible stars, but a substantial fraction is likely to be in the form of dark matter [Casertano *et al.*, 1993]. This dark matter should be in another Universe than ours.

3. Historically, the prediction of Halley's Comet bas always been errors of 3 or 4 days in the predicted time of the perihelion passage. Joseph Brady, the scientist of California Institute of Technology, based on studies of periods of Halley's Comet using old European and Chinese records, and used a computer to treat the data of it in a numerical model of the solar system, he has been able to predict an invisible X planet (trans-plutonian planet), which was about three times the size of Saturn with highly inclined orbit (i=120°, e= ± 0.07) to the ecliptic and the time period of it to be 450 years [Brady, 1971,1972]. Flandern (1981) proposed a search for an X planet, which has about three times the mass of the Earth and a highly inclined eccentric orbit that accounted for all of the perturbations on the motions of Neptune. Anderson (1988), NASA research scientist, presented the deviation of Neptune and Uranus in the regular orbit and proposed “The Theory of X Planet” from observed astronomical data of the nineteen century. The mass of X planet is about five times that of the Earth and its period is about 700～1000 years. The orbit is elliptical and the inclination from the orbit to ecliptics very large and almost perpendicular. Now the planet X has been searched for, but it still remains to be found. If the dark planet X orbits around the Sun in the other Universe than ours, then its gravity will sometimes affect the motion of Halley's Comet, Neptune and Uranus. Therefore, the problem of the invisible planet X may be solved.

This is absolutely a new try to break the bottlenecks of the research in the deep interior of the Earth in the geophysics and in the spaces of the Universe in the astrophysics. From the applications of the ten-dimensional space-time of String theory, the three-cosmic framework of the Universes is inferred. Some scientific problems of the geophysics and astrophysics may be roughly solved as above, but that still needs to be proved by the fine outcomes of physicists' new research.

ACKNOWLEDGEMENT

I am grateful to Dr. Lin-Gun Liu of Research School of Earth Science in Australian for constructive criticisms and helpful comments in 1990.

REFERENCES

Ade, P.A.R., Aghanim, N., Armitage-Caplan, C. *et al*. (Planck Collaboration), 2014. Planck 2013 results. I. Overview of products and scientific results, *Astronomy & Astrophysics*, 5 Jun 2014.

Agnew, D., Berger, J., Buland, R., Farrell, W. & Gilbert, F., 1976. International Deployment of Accelerometers: a

network for very long period seismology, *EOS, Trans. Am. Geophys. Union,* **57**, 180–188.

Ahrens, T.J., 1980. Dynamic Compression of Earth Materials, *Science* **207**, 1035.

Alboussière, T., Deguen, R. & Melzani, M., 2010. Melting-induced stratification above the Earth's inner core due to convective translation. *Nature* 466, 744–747.

Altshuler, L.V. & Sharipdzhanov, L.V., 1971. On the distribution of iron in the Earth, the chemical distribution of the latter. *Bull. Acad. Sci. USSR, Geophys. Ser.*, **4**, 3–16.

Anderson, John, 1988. Planet X - Fact or Fiction? *Planetary Report*, **8**, (4), 6–9.

Anzellini, S., Dewaele, A., Mezouar, M., Loubeyre, P. & Morard, G., 2013. Melting of Iron at Earth's Inner Core Boundary Based on Fast X-ray Diffraction, *Science,* **340**, (6131), 464–466.

Araki, T. *et al*. (KamLAND Collaboration), 2005. Experimental investigation of geologically produced antineutrinos with KamLAND, *Nature*, **436**, 499–503.

Aubert, J., Amit, H., Hulot, G. & Olson, P., 2008. Thermochemical flows couple the Earth's inner core growth to mantle heterogeneity, *Nature,* **454,** 758–762.

Bartusiak, Marcia, 1988. Wanted: Dark Matter, *Discover*, Dec. 1988. 63–69.

Basu A.R., Poreda R.J., Renne P.R., Teichmann F., Vasiliev Y.R., Sobolev N.V. & Turrin B.D., 1995. High ^{3}He plume origin and temporal-spatial evolution of the Siberian flood basalts, *Science*, **269**, 822–825.

Bellini, G. *et al*. (Borexino Collaboration), 2010. Observation of geo-neutrinos, *Phys. Lett.* B, **687**, 4–5, 299–304.

Bennett, C.L. *et al*., 2013. Nine-year Wilkinson Microwave Anisotropy Probe (WMAP) Observations: Final Maps and Result. *The Astrophysical Journal Supplement,* **208**, (2), 20.

Bergman, M.I., 2003. Solidification of the Earth's core, in Earth's Core: Dynamics, Structure, Rotation, *Geodyn. Ser.,* 105–127.

Birch, Francis, 1939. The variation of seismic velocities within a simplified earth model in accordance with the theory of finite strain, *Bull. Seismol. Soc. Amer.*, **29**, 463-479.

Bloxham, J. & Gubbins, D., 1987. Thermal core-mantle interactions. *Nature*, **325**: 511–513.

Bloxham, J. & Jackson, A., 1990. Lateral temperature variations at the core-mantle boundary deduced from the magnetic field, *Physical Review Letters*, **17**, No. 11, 1997–2000.

Blumenthal, G.R., Faber, S.M., Primack, J.R. & Rees, M.J., 1984. Formation of galaxies and large-scale structure with cold dark matter. *Nature*, **311**, 517–525.

Bolt, Bruce A. & Qamar, A., 1970. Upper bound to the density jump at the boundary of the Earth's inner core, *Nature*, **228**, 148–150.

Bolt, Bruce A., 1972. The density distribution near the base of the mantle and near the Earth's center, *Phys. Earth Planet. Inter.*, **5**, 301–311.

Boschi, L. & Dziewonski, A.M., 1999. High and low resolution images of the Earth's mantle: Implications of different approaches to tomographic modeling, *J. Geophys. Res*., **104**, (B11), 25567–25594.

Boschi, L. & Dziewonski, A.M., 2000. Whole Earth tomography from delay times of *P*, *PcP*, and *PKP* phases

lateral heterogeneities in the outer core or radial anisotropy in the mantle? *J. Geophys. Res.* **105**, 13675–13696.

Bowin, C., 1986. Topography at the core mantle boundary, *Geophys. Res. Lett.,* **13,** 1513–1516.

Brady, Joseph L., 1971. The orbit of Halley's Comet and apparition of 1896, *Astronomical Journal,* **76**, No. 8. 728–739.

Brady, Joseph L., 1972.The Effect of Trans-plutonian Planet on Halley's Comet. *Publication of the Astronomical Society of the Pacific.* **34**. No. 498, 314–322.

Buchbinder, G.G.R., 1968. Properties of the Core-Mantle Boundary and Observations of PcP, *J. Geophys. Res*., **73**, 5901.

Bullen, K.E. & Bolt, B.A., 1986. An Introduction to the Theory of Seismology, 4th Ed., *Geophysical Journal of the Royal Astronomical Society,* **86**, 1, 215–216.

Byrne, Peter, 2008. The Many Worlds of Hugh Everett**,** *Scientific American,* on October 21, 2008.

Casertano, S., Iben, I. & Shilds, A., 1993.The Hyades Cluster-Supercluster Connection: Evidence for a Local Concentration of Dark Matter, *Astrophysical Journal*. Part 1, **410**, 90-98.

Chandler, S. C., 1891. On the variation of latitude, *Astronomical Journal*, **11**, 59-61, 65-70.

Choy, G.L. & Cormier, V.F., 1983. The structure of the inner core inferred from short-period and broad-band GDSN data, *Geophys. J. R. Astr. Soc*., **72**, 1–21.

Condie, Kent C., 1997. Plate tectonics and crustal evolution (4th Ed.). *Butterworth-Heinemann*, p. 5.

Cormier, V.F., 1981. Short-period PKP phases and the inelastic mechanism of the inner core, *Phys. Earth Plant. Inter*. **24**, 291–301.

Cormier, V.F., 2009. A glassy lowermost outer core. *Geophys. J. Int*. **179**, 374–380.

Cormier, V.F., Attanayake, J. & He, K., 2011. Inner core freezing and melting: constraints from seismic body waves. *Phys. Earth Planet. Inter*. **188**, 163–172.

Creager, K.C. & Jorden, T.H., 1986. Aspherical structure of the core-mantle boundary from PKP travel time, *Geophysics. Res. Lett*., **13**, 1497–1500.

Davies, J.H. & Davies, D.R., 2010. Earth's surface heat flux, *Solid Earth*, **1**, 5–24.

Davies, J.H., 2013: Global Surface Heat Flow Map, *Geophysical Research Abstracts,* **15**, EGU2013–10885.

Derr, J.S., 1969. Internal Structure of the Earth Inferred from Free Oscillations, *J. Geophysics. Res*., **74**, 5202–5220.

Doornbos, D.J., 1978. On seismic-wave scattering by rough core–mantle boundary, *Geophys. J. R. astr. Soc.*, **53**, 643–662.

Doornbos, D.J. & Hilton, T., 1989. Models of the core-mantle boundary and the travel times of internally reflected core phases, *J. Geophys. Res*., **94**, B11, 15,741–15,751.

Dvali, Georgi, 2004. Out of the Darkness, *Scientific American*, February, 68–75.

Dye, S.T., 2012. Geoneutrinos and the radioactive power of the Earth. *Reviews of Geophysics*, 50, RG3007, 1-19.

Dziewonski, A.M. & Anderson, D.L., 1981. Preliminary Reference Earth Model, *Phsy. Earth Planet, Inter*., **25**, 297–356.

Dziewonski, A.M. & Woodhouse, J.H., 1987. Global Images of the Earth's Interior, *Science*, **236**, No. 4797, 37–48.

Earle, P.S. & Shearer, P.M., 1997. Observations of PKKP precursors used to estimate small-scale topography on the core-mantle boundary, *Science*, **277**, 667–670.

Engdahl, E.R., van der Hilst, R. & Buland, R., 1998. Global teleseismic earthquake relocation with improved travel time and procedures for depth determination. *Bull. Seism. Soc. Am*. **88**, 722–743.

Everett, Hugh, 1957. Relative State Formulation of Quantum Mechanics. *Reviews of Modern Physics.* **29**, 454–462.

Fiorentini, G., Lissia, M. & Mantovani, F., 2007. Geo-neutrinos and Earth's interior, *Phys. Rep.*, **453**, 117–172.

Fiquet, G., Auzende, A.L., Siebert, J., Corgne, A., Bureau, H., Ozawa, H. & Garbarino, G., 2010. Melting of peridotite to 140 gigapascals. *Science*, **329,** 1516–1518.

Fermi, E., 1947. Nuclear reactor theory, *Science* **105,** 27–32.

Flandern, T.V., 1981. The renewal of the Trans-Neptunian planet search, *Bulletin of the American Astronomical Society* **12**, 830.

Forte, A.M., Mitrovica, J.X. & Woodward, R.L., 1995. Seismic-geodynamic determination of the origin of excess ellipticity of the core-mantle boundary, *Geophys. Res. Lett.*, **22**, (9), 1013–1016.

Forte, A.M. & Peltier, R.W., 1991. Mantle convection and core-mantle boundary topography: Explanations and implications, *Tectonophysics*, **187**, (1–3), 91–116.

Gando, A., Dwyer, D.A., McKeown, R.D., Zhang, C., 2011. Partial radiogenic heat model for Earth revealed by geoneutrino measurements, *Nat. Geosci.*, **4**, 647–651.

Garland, G. D., 1979. Introduction to Geophysics. 2nd ED., *W. B. Saunders Company*, Toronto, Canada. 4-8, 28-30, 44-46, 130, 387-389.

Garcia, R. & Souriau, A., 2000. Amplitude of the core–mantle boundary topography estimated by stochastic analysis of core phases. *Phys. Earth Planet. Inter*. **117**, 345–359.

Gross, Richard S., 2000. The Excitation of the Chandler Wobble, *Geophysical Research Letters*, **27**, (15), 2329–2332.

Gubbins, D. & Richards, M.A., 1986. Coupling of the core dynamo and mantle: Thermal or Topography? *Physical Review Letters*, **13**, 1521–1524.

Gubbins, D. & Masters, T.G., 1979. *Adv. Geophys.* **59**, 57–99.

Gubbins, D., Masters, T.G. & Nimmo, F., 2008. A thermochemical boundary layer at the base of Earth's outer core and independent estimate of core heat flux, *Geophys. J. Int.*, **174**, 1007–1018.

Gundmundsson, O., Clayton, R.W. & Anderson, D.L., 1986. CMB topography inferred from ISC PcP *travel times, EOS, Trans. AGU, **67**, 1100.*

Gwinn, C.R., Herring, T.A. & Shapiro, I.I., 1986. Geodesy by radio interferometry: studies of the forced nutations of the Earth – 2. Interpretation, *J. geophys. Res.*, **91**, 4755–4765.

Hagemann, R. & Roth, E., 1978. Relevance of the studies of the Oklo natural reactors to the storage of radioactive wastes. *Radiochemica Acta*, **25**, 241–247.

Hager, B.H., Clayton, R.W., Richards, M.A., Comer, R.P. & Dziewonski, A.M., 1985. Lower mantle heterogeneity, dynamic topography and the geoid, *Nature*, **313**, 541–546.

Hall, T.H. & Murthy, V.R., 1972. Comments on the Chemical Structure of a Fe-Ni-S Core of the Earth, *EOS*. **53**, No.5, 602.

Hand, E., 2015. Mantle plumes seen rising from Earth's core, *science*, **349**, 6252, 1032–1033.

Hecht, J., 1995. Buried treasure from hot heart of the Earth, *New Scientist*, **19**, 16,

Ho, Hsien-Jung, 1993. Reconstruction of the Earth Model and Discovery of the Interior Dark Matter, *First Symposium on UFO cross-strait. China Ufology Institute*, http://newidea.org.tw/PDF/S2.pdf.

Hollenbach, D.F. & Herndon, J.M., 2001. Deep-earth reactor: nuclear fission, helium, and the geomagnetic field. *Proc. Nat. Acad. Sci. USA*, **98**, 20, 11085–11090.

Javoy, M., 1999. Chemical Earth models. Comptes Rendus de l'Acadēmie des Sciences Series II A *Earth and Planetary Science*, **329**, 537–555.

Jaupart, C., Labrosse, S. & Mareschal, J.C. 2007.Temperature, heat and energy in the mantle of the Earth, *Geophysics*, **7**, 253–303.

Jeanloz, R. & Ahrens, T.J., 1980. Equations of FeO and CaO, *Geophysics. J. R. Astr. Soc*, **62**, 505–528.

Jeanloz, R. & Wenk, H.R., 1988. Convection and anisotropy of the inner core, *Geophysics. Res. Lett*. **15**, 72–75.

Jeanloz, R., 1990. The Nature of the Earth's Core, *Annual Review of Earth and Planetary Sciences*, **18**: 357-386

Jeffreys, H., 1939. The times of the core waves, *Mon. Not. R. Astron. Soc. Geophys. Suppl.*, **4**, 498.

Jephcoat, A. & Olson, P., 1987. Is the Inner Core of the Earth Pure Iron? *Nature*, **325**, 332–335.

Kaku, M., 1988. Introduction to Superstrings, *Springer Verlag New York Inc*., New York, USA. 16–18.

Kaula, W.M., Sleep, N.H. & Phillips, R.J., 1989. More about the Moment of Inertia of Mars, *Geophysical Research Letters*, 16, No. 11, 1333-1336.

Kennett, B.L.N., Engdahl, E.R. & Buland, R., 1995. Constraints on seismic velocities in the Earth from travel times, *Geophys. J. Int*., **122**, 108– 124.

Kerr, Richard A., 1997. Deep-Sinking Slabs Stir the Mantle. *Science. AAAS.* Retrieved 2013-06-13.

Knittle, E. & Jeanloz, R., 1991. The high-pressure phase diagram of $Fe_{0.94}O$：A possible constituent of the Earth's core, *J. Geophysics. Res.*, **96**, 16169–16180.

Knopoff, F., 1965. A preeminent seismology, *Phys. Rev*., **138** A, 1445.

Koelemeijer, P.J., Deuss, A. & Trampert J., 2012. Normal mode sensitivity to Earth's D'' layer and topography on the core-mantle boundary: what we can and cannot see**.** *Geophys. J. Int.*, **190,** 553–568.

Koper, K.D., Pyle, M.L. & Franks, J.M., 2003. Constraints on aspherical core structure from *PKiKP-PcP* differential travel times, *J. Geophys. Res.*, **108**, (B3), 2168.

Korenaga, J., 2008. Urey ratio and the structure and evolution of Earth's mantle, *Reviews of Geophysics*, **46**, (2), June 2008.

Kubala, Bizy, & Mahan Rao, 1996. Earth's Core Temperature. *Byrdand Black*.

Kuroda, P.K., 1956. On the Nuclear Physical Stability of the Uranium Minerals. *Journal of Chemical Physics* **25** (4): 781–782; 1295–1296.

Lay, T., 1989. Structure of the Core-Mantle Transition Zone: A Chemical and Thermal Boundary Layer, *EOS*, **70**, No. 4, Jan. 24, 49, 54–55, 58–59.

Lay, T., Hernlund, J. & Buffett, B.A., 2008. Core–mantle boundary heat flow. *Nature Geoscience*, **1**, (1), 25–32.

Liu, Lin-Gun, 1974. Birch's Diagram; some new observations, *Phys. Earth Planet inter*., **8**, 56–62.

Lubin, P.M., Bond, J R., Efstathiou, G. & Meinhold, P.R., 1991. Cosmic-Structure Constraints from a One-Degree Microwave-Back-ground Anisotropy Experiment. *Physical Review Letters*, **66**, 2179–2182.

Lyttleton, R.A., 1973. The end of the iron-core age, *Moon*, **7**, 422–439.

McFadden, Phillip L. & Merrill Ronald T., 1995. History of Earth's magnetic field and possible connections to core-mantle boundary processes. *J. Geophysics. Res*., **100**, 307–316.

McQueen, R.G., Marsh, S.P., Taylor, J.W., Fritz, J.N. & Carter, W.J., 1970. The equation of state of solids from shock wave studies, in high velocity impact phenomena, Kinslow, R., Academic Press, New York, 294–419.

Meshik, A.P., Hohenberg, C.M. & Pravdivtseva, O.V., 2004. Record of cycling operation of the natural nuclear reactor in the Oklo/Okelobondo area in Gabon. *Phys. Rev. Lett.*, **93**, 182302.

Mjelde, R. & Faleide, J.I., 2009. Variation of Icelandic and Hawaiian magmatism: evidence for co-pulsation of mantle plumes? *Mar. Geophys. Res.*, **30**, 61–72.

Mjelde, R., Wessel, P. & Müller, D., 2010. Global pulsations of intraplate magmatism through the Cenozoic. *Lithosphere*, **2**, (5), 361–376.

Morelli, A. & Dziewonski, M., 1987. Topography of the core-mantle boundary and lateral homogeneity of the liquid core, *Nature*, **325**, 19, Feb., 678–683.

Morgan, W.J., 1971. Convection plumes in the lower mantle: *Nature*, **230**, 42–43.

Morgan, W.J., 1972. Deep mantle convection plumes and plate motions, *Bull. Am. Assoc. Pet. Geol.* **56**, 203–213.

Neuberg, J. & Wahr, J., 1991. Detailed investigation of a spot on the core mantle boundary using digital PcP data, *Phys. Earth planet. Inter.*, **68,** 132–143.

Obayashi, M. & Fukao, Y., 1997. *P* and *PcP* travel time tomography for the core–mantle Boundary. *J. Geophys. Res*. **102**, 17825–17841.

Peji*ć*, T. & Tkal*č*i*ć*, H., 2016. Toward attenuation tomography of the uppermost inner core from PKP waves,

Geophysical Research Abstracts, **18**, EGU 2016–1605.

Perlmutter, S.; Aldering; Goldhaber; Knop; Nugent; Castro; Deustua; Fabbro; Goobar; Groom; Hook; Kim; Kim; Lee; Nunes; Pain; Pennypacker; Quimby; Lidman; Ellis; Irwin; McMahon; Ruiz-Lapuente; Walton; Schaefer; Boyle; Filippenko; Matheson; Fruchter; *et al*., 1999. Measurements of Omega and Lambda from 42 high redshift supernovae. *Astrophysical Journal*, **517**, (2), 565–86.

Peterson, J., Butler, H.M., Holcomb, L.G. & Hutt, C.R., 1976. The seismic research observatory, *Bull. Seism. Soc. Am.* **66**, 2049–2068.

Pollack, H.N., Hurter, S.J. & Johnson, J.R., 1993. Heat flow from the Earth's interior: Analysis of the global data set, *Rev. Geophys.*, **31**, 267–280.

Puchkov, V.N., 2009. The Controversy over Plumes: Who Is Actually Right? *Geotectonics*, **43**, No.1, 1–17.

Qamar, A., 1973. Revised velocities in the Earth's core, *Bull. Seismol. Soc. Am*., **63**, 1073– 1105.

Ramsey, W.H., 1948. On the constitution of the terrestrial planets, *Mon. Not. Roy. Astron. Soc*., **108**, 406–413.

Rial, J.A. & Cormier, V.F., 1980. Seismic waves at the Epicenter's antipodes, *J. Geophysics. Res*., **91**, 10203–10228.

Riess Adam G. *et al*., (High-z Supernova Search Team),1998. Observational Evidence from Supernovae for an Accelerating Universe and a Cosmological Constant. *Astronomical Journal*, **116**, No. 3, 1009–1038

Ringwood, A.E., 1984. The Earth's Core: its composition, formation and bearing upon the origin of the Earth, *Proc. R. Soc*. A, **395**, 1–46.

Rodgers, A. & Wahr, J., 1993. Inference of core–mantle boundary topography from ISC *PcP* and *PKP* travel times. *Geophys. J. Int*. **115**, 991–1011.

Ruff, L. & Anderson, D.L., 1980. Core formation, evolution, and convection: A geophysical model, *Phys. Earth Planet. Inter.*, **21,** 181-201.

Sawangwit, U. & Shanks, T., 2010. Durham astronomers' doubts about the 'dark side', *Royal Astronomical Society NEWS & PRESS*, 15. June 2010.

Schlaphorst, D., Thomas, C., Holme, R. & Abreu, R., 2016. Investigation of core–mantle boundary topography and lowermost mantle with P4KP waves, *Geophysical Journal International* **204**, (2), 1060-1071.

Scherk, J. & Schwarz, J.H., 1975. Dual field theory of quarks and gluons, *Physics Letters*, **57,** B, 463–466.

Schwarz, J.H. & Scherk, J., 1974. Dual models for non-hadrons. *Nuclear Physics*, B, **81**, 118-144.

Shearer, P. & Masters, G., 1990. The density and shear velocity contrast at the inner core boundary, *Geophysics. J. Int.*, **102**, 491–498.

Shimizu, H., Poirier, J.P. & Le Mouël, J.L., 2005. On crystallization at the inner core boundary. Phys. *Earth Planet. Inter*. **151**, 37–51.

Siegfried, T., 1999. Hidden Space Dimensions May Permit Parallel Universes, Explain Cosmic Mysteries. *The Dallas Morning News*, 5 July 1999.

Singh, S.C., Taylor, M.A.J. & Montagner, J.P., 2000. On the presence of liquid in Earth's inner core. *Science*

287: 2471–2474.

Soldati, G., Koelemeijer, P., Boschi, L. & Deuss A., 2013. Constraints on core-mantle boundary topography from normal mode splitting, *Geochem. Geophys. Geosyst.* 14.

Soldati, G., Boschi, L., Mora, S.D. & Forte, A.M., 2014. Tomography of core-mantle boundary and lowermost mantle coupled by geodynamics: joint models of shear and compressional velocity, Annals of Geophysics, **57**, No 6.

Song, X. & Helmberger, Don V., 1995. A P wave velocity model of earth's core, *J. Geophysics., Res*., **100**, No. B7, 9817–9830.

Song, X. & Dai, W., 2008. Topography of Earth's inner core boundary from high-quality waveform *Geophysical Journal International*, **175**, (1), 386–399.

Souriau, A. & Souriau, M., 1989. Ellipticity and density at the inner core boundary from subcritical PKiKP and PcP data, *Geophysics. J. Int*., **98**, 39–54.

Souriau, A. & Poupinet, G., 1991. The velocity profile at the base of the liquid core from PKP (BC + Cdiff) data: An argument in favor of radial inhomogeneity, *Geophys. Res. Lett.*, **18**, 2023–2026.

Steinberger, B. & Holme, R., 2002. Mantle flow models with core-mantle boundary constraints, paper presented at 8th Symposium of the Study of Earth's Deep Interior, *Int. Union of Geod. and Geophys*., Lake Tahoe, Calif., 22 – 26 July.

Steinberger, B. & Holme, R., 2008. Mantle flow models with core-mantle boundary constraints and chemical heterogeneities in the lowermost mantle, *J. Geophys. Res*., **113**, B05403.

Stevenson, D.J., 1987. Limits on lateral density and velocity variations in the Earth's outer core, *Geophysics. J. R. Astr. Soc*., **88**, 311–319.

Stokes, G.M. & Michalsky, J.J., 1979. Cygnus X-1, Mercury **8**, 60.

Stsrobinskii A.A. & Zel'dovich, Za. B., 1988. Quantum Effects in Cosmology, *Nature* **331**, 25.

Sumita, I. & Olson, P., 1999. A laboratory model for convection in Earth’s core driven by a thermally heterogeneous mantle. *Science* **286**, 1547–1549.

Sumita, I. & Olson, P., 2002. Rotating thermal convection experiments in a hemispherical shell with heterogeneous boundary heat flux: implications for the Earth’s core. *J. Geophys. Res*. **107**, 2169.

Sze, E.K.M. & van der Hilst, R.D., 2003. Core mantle boundary topography from short period *PcP*, *PKP* and *PKKP* data**,** *Physics of the Earth and Planetary Interiors*, **135**, 27–46.

Tanaka, S., 2010. Constraints on the core-mantle boundary topography from P4KP-PcP differential travel times, *J. geophys. Res.: Solid Earth*, 115.

Van Schmus, W.R., 1995. Natural radioactivity of the crust and mantle, *Global Earth Physics: A Handbook of Physical Constants*, 283–291.

Walker R.J. & Morgan J.W., Horan M.F., 1995. Osmium-187 in some plumes: Evidence for core-mantle interaction? *Science*, **269**, 819–822.

Waszek, L. & Deuss, A., 2015a. Observations of exotic inner core waves, *Geophys. J. Int*., **200**, (3): 1636–

1650.

Waszek, L. & Deuss, A., 2015b. Anomalously strong observations of *PKiKP/PcP* amplitude ratios on a global scale, *J. Geophys. Res. Solid Earth*, 120.

Witten, Edward, 1995. String theory dynamics in various dimensions, *Nuclear Physics,* B. **443**, 85.

Witten, Edward, 1998. Magic, Mystery and Matrix, *Notices of the AMS,* October 1998, 1124–1129.

Woit, Peter, 2013. The "Dark Flow" & Existence of Other Universes ─New Claims of Hard Evidence, *New Scientist*, June 03, 2013.

Woodhouse, J.H. & Dziewonski, A.M., 1989. Seismic modeling of the Earth's large-scale three-dimensional structure, *Phil. Trans. R. Soc. Lond*. A 328, 291–308.

Yoshida, M., 2008. Core–mantle boundary topography estimated from numerical simulations of instantaneous flow. *Geochem. Geophys. Geosys*. **9**, (7).

Young, C.J. & Lay, T., 1987. The core–mantle boundary, *Ann. Rev. Earth Planet. Sci*., **15**, 25–46.

Yu, W., Wen, L. & Niu, F., 2005. Seismic velocity structure in the Earth's outer core, *J. Geophys. Res.*, **110**, B02302.

Zou, Z., Koper, K.D. & Cormier, V.F., 2008. The structure of the base of the outer core inferred from seismic waves diffracted around the inner core, *J. Geophys. Res*., **113**, B05314.

Zwicky, F., 1937. On the Masses of Nebulae and of Clusters of Nebulae. *Astrophysical Journal*, **86**, 217.

ATTACHMENTS

Table 2. The calculated data of the PREM from the simplified method.

Level	Radius R	Density ρ	Mass of Shell M	Moment of Inertia I	Gravity g	Pressure P
No.	km	g/cm^2	10^{24} g	10^{40} g.cm^2	10^3·cm/s^2	kbar
94	6371.0	1.02000	5973.289	80205.664	981.959	0.000
93	6368.0	1.02000	5971.729	80163.472	982.628	0.301
92	6368.0	2.60000	5971.729	80163.472	982.628	0.301
91	6356.0	2.60000	5955.860	79735.267	983.721	3.368
90	6356.0	2.90000	5955.860	79735.267	983.721	3.368
89	6346.6	2.90000	5942.042	79363.655	984.348	6.051
88	6346.6	3.38076	5942.042	79363.655	984.348	6.051
87	6331.0	3.37906	5915.418	78650.501	984.772	11.242
86	6311.0	3.37688	5881.498	77746.958	985.341	17.897
85	6291.0	3.37471	5847.813	76855.371	985.937	24.552
84	6291.0	3.37471	5847.813	76855.371	985.937	24.552
83	6256.0	3.37091	5789.430	75323.498	987.046	36.197
82	6221.0	3.36710	5731.761	73827.216	988.241	47.843
81	6186.0	3.36330	5674.801	72365.862	989.523	59.490
80	6151.0	3.35950	5618.547	70938.843	990.895	71.140
79	6151.0	3.43578	5618.547	70938.843	990.895	71.140
78	6106.0	3.46264	5545.290	69104.504	992.443	86.533
77	6061.0	3.48951	5472.542	67309.578	994.021	102.070
76	6016.0	3.51639	5400.312	65553.702	995.631	117.752
75	5971.0	3.54325	5328.609	63836.530	997.275	133.580
74	5971.0	3.72378	5328.609	63836.530	997.275	133.580
73	5921.0	3.78678	5245.188	61870.242	998.311	152.315
72	5871.0	3.84980	5161.788	59937.364	999.243	171.384
71	5821.0	3.91282	5078.443	58038.407	1000.070	190.784
70	5771.0	3.97584	4995.188	56173.776	1000.794	210.515
69	5771.0	3.97584	4995.188	56173.776	1000.794	210.515
68	5736.0	3.98399	4937.243	54894.999	1001.293	224.460
67	5701.0	3.99214	4879.884	53644.500	1001.849	238.440
66	5701.0	4.38071	4879.884	53644.500	1001.849	238.440
65	5650.0	4.41241	4789.122	51695.390	1001.046	260.896
64	5600.0	4.44316	4701.095	49838.510	1000.272	283.051
63	5600.0	4.44317	4701.095	49838.510	1000.272	283.051
62	5500.0	4.50372	4527.934	46282.178	998.780	327.772
61	5400.0	4.56307	4358.719	42930.977	997.393	373.027
60	5300.0	4.62129	4193.543	39778.675	996.149	418.809
59	5200.0	4.67844	4032.484	36818.780	995.087	465.113
58	5100.0	4.73460	3875.615	34044.639	994.249	511.936
57	5000.0	4.78983	3722.994	31449.399	993.682	559.281
56	4900.0	4.84422	3574.669	29026.105	993.433	607.151
55	4800.0	4.89783	3430.681	26767.722	993.557	655.550
54	4700.0	4.95073	3291.058	24667.171	994.111	704.504
53	4600.0	5.00299	3155.823	22717.392	995.158	754.016
52	4500.0	5.05469	3024.990	20911.315	996.768	804.113
51	4400.0	5.10590	2898.564	19241.931	999.016	854.820
50	4300.0	5.15669	2776.543	17702.299	1001.988	906.171
49	4200.0	5.20713	2658.919	16285.574	1005.777	958.203
48	4100.0	5.25729	2545.676	14985.041	1010.487	1010.963

Level	Radius R	Density ρ	Mass of Shell M	Moment of Inertia I	Gravity g	Pressure P
No.	km	g/cm^2	10^{24} g	10^{40} $g.cm^2$	$10^3 \cdot cm/s^2$	kbar
47	4000.0	5.30724	2436.792	13794.099	1016.234	1064.504
46	3900.0	5.35706	2332.241	12706.303	1023.150	1118.888
45	3800.0	5.40681	2231.989	11715.364	1031.383	1174.188
44	3700.0	5.45657	2135.997	10815.178	1041.100	1230.486
43	3630.0	5.49145	2071.317	10235.887	1048.886	1270.533
42	3630.0	5.49145	2071.317	10235.887	1048.886	1270.533
41	3600.0	5.50642	2044.225	9999.856	1052.492	1287.866
40	3500.0	5.55641	1956.620	9263.582	1065.775	1346.464
39	3480.0	5.56645	1939.595	9125.339	1068.680	1358.335
38	3480.0	9.90349	1939.595	9125.339	1068.680	1358.335
37	3400.0	10.02940	1821.025	8189.719	1051.122	1442.882
36	3300.0	10.18134	1678.502	7123.015	1028.464	1548.038
35	3200.0	10.32726	1542.384	6164.138	l005.050	1652.385
34	3100.0	10.46727	1412.729	5306.115	980.913	1755.720
33	3000.0	10.60152	1289.573	4541.998	956.089	1857.844
32	2900.0	10.73012	1172.922	3864.903	930.611	1958.564
31	2800.0	10.85321	1062.760	3268.068	904.512	2057.694
30	2700.0	10.97091	959.048	2744.899	877.825	2155.056
29	2600.0	11.08335	861.725	2288.994	850.584	2250.478
28	2500.0	11.19067	770.709	1894.191	822.821	2343.794
27	2400.0	11.29298	685.901	1554.580	794.573	2434.847
26	2300.0	11.39042	607.181	1264.538	765.875	2523.487
25	2200.0	11.48311	534.411	1018.739	736.758	2609.572
24	2100.0	11.57119	467.440	812.171	707.265	2692.969
23	2000.0	11.65478	406.100	640.145	677.436	2773.552
22	1900.0	11.73401	350.208	498.303	647.312	2851.205
21	1800.0	11.80900	299.568	382.619	616.944	2925.821
20	1700.0	11.87990	253.973	289.403	586.388	2997.305
19	1600.0	11.94682	213.202	215.291	555.708	3065.572
18	1500.0	12.00989	177.026	151.249	524.988	3130.550
17	1400.0	12.06924	145.204	112.556	494.331	3192.185
16	1300.0	12.12500	117.486	78.802	463.868	3250.438
15	1221.5	12.16634	98.436	58.583	440.212	3293.691
14	1221.5	12.16360	98.436	58.583	440.212	3293.691
13	1200.0	12.77493	93.378	53.640	432.690	3305.677
12	1100.0	12.82501	72.093	34.814	397.560	3359.210
11	1000.0	12.87073	54.279	21.671	362.182	3408.454
10	900.0	12.91211	39.646	12.826	326.595	3453.339
9	800.0	12.94912	27.892	7.132	290.800	3493.806
8	700.0	12.98178	18.714	3.665	254.839	3529.806
7	600.0	13.01009	11.800	1.698	218.713	3561.307
6	500.0	13.03404	6.836	0.684	182.456	3588.295
5	400.0	13.05364	3.503	0.224	146.088	3610.792
4	300.0	13.06888	1.479	0.054	109.653	3628.883
3	200.0	13.07977	0.438	0.007	73.065	3642.820
2	100.0	13.08630	0.055	0.001	36.699	3653.579
1	0.0	13.08848	0.000	0.000	0.000	3655.973

Table 4. The pressure P of the PREM and the deviation E of the calculated pressure of simplified method from the value of P.

Layer	Radius	Simplified Method P	Pressure of PREM	deviation E
	km	kbar	kbar	
94	6371	0	0	0
93	6368	0.301	0.299	0.006688963
92	6368	0.301	0.303	-0.00660066
91	6356	3.368	3.364	0.001189061
90	6356	3.368	3.37	-0.000593472
89	6346.6	6.051	6.04	0.001821192
88	6346.6	6.051	6.043	0.001323846
87	6331	11.242	11.239	0.000266928
86	6311	17.897	17.891	0.000335364
85	6291	24.552	24.539	0.000529769
84	6291	24.552	24.546	0.000244439
83	6256	36.197	36.183	0.000386922
82	6221	47.843	47.824	0.00039729
81	6186	59.49	59.466	0.000403592
80	6151	71.14	71.108	0.00045002
79	6151	71.14	71.115	0.000351543
78	6106	86.533	86.497	0.000416199
77	6061	102.07	102.027	0.000421457
76	6016	117.752	117.702	0.000424802
75	5971	133.58	133.52	0.000449371
74	5971	133.58	133.527	0.000396923
73	5921	152.315	152.251	0.000420358
72	5871	171.384	171.311	0.000426126
71	5821	190.784	190.703	0.000424744
70	5771	210.515	210.425	0.000427706
69	5771	210.515	210.426	0.000422952
68	5736	224.46	224.364	0.000427876
67	5701	238.44	238.334	0.000444754
66	5701	238.44	238.342	0.000411174
65	5650	260.896	260.783	0.00043331
64	5600	283.051	282.927	0.000438276
63	5600	283.051	282.928	0.00043474
62	5500	327.772	327.623	0.000454791
61	5400	373.027	372.852	0.000469355
60	5300	418.809	418.606	0.000484943
59	5200	465.113	464.882	0.0004969
58	5100	511.936	511.676	0.000508134
57	5000	559.281	558.991	0.000518792
56	4900	607.151	606.83	0.000528978
55	4800	655.55	655.202	0.000531134
54	4700	704.504	704.119	0.000546783
53	4600	754.016	753.598	0.000554672
52	4500	804.113	803.66	0.000563671
51	4400	854.82	854.332	0.000571207
50	4300	906.171	905.646	0.000579697
49	4200	958.203	957.641	0.000586859
48	4100	1010.963	1010.363	0.000593846
47	4000	1064.504	1063.864	0.000601581
46	3900	1118.888	1118.207	0.000609011
45	3800	1174.188	1173.465	0.000616124
44	3700	1230.486	1229.719	0.00062372
43	3630	1270.533	1269.741	0.000623749

42	3630	1270.533	1269.742	0.000622961
41	3600	1287.866	1287.067	0.000620791
40	3500	1346.464	1345.619	0.000627964
39	3480	1358.335	1357.509	0.000608467
38	3480	1358.335	1357.51	0.00060773
37	3400	1442.882	1441.941	0.000652593
36	3300	1548.038	1546.982	0.000682619
35	3200	1652.385	1651.209	0.000712205
34	3100	1755.72	1754.418	0.000742126
33	3000	1857.844	1856.409	0.000772998
32	2900	1958.564	1956.991	0.000803785
31	2800	2057.694	2055.978	0.000834639
30	2700	2155.056	2153.189	0.000867086
29	2600	2250.478	2248.453	0.000900619
28	2500	2343.794	2341.603	0.000935684
27	2400	2434.847	2432.484	0.000971435
26	2300	2523.487	2520.942	0.001009543
25	2200	2609.572	2606.838	0.00104878
24	2100	2692.969	2690.035	0.001090692
23	2000	2773.552	2770.407	0.001135212
22	1900	2851.205	2847.839	0.001181949
21	1800	2925.821	2922.221	0.00123194
20	1700	2997.305	2993.457	0.00128547
19	1600	3065.572	3061.461	0.001342823
18	1500	3130.55	3126.159	0.001404599
17	1400	3192.185	3187.493	0.001472003
16	1300	3250.438	3245.423	0.001545253
15	1221.5	3293.691	3288.502	0.001577922
14	1221.5	3293.691	3288.513	0.001574572
13	1200	3305.677	3300.48	0.001574619
12	1100	3359.21	3353.596	0.001674024
11	1000	3408.454	3402.383	0.001784338
10	900	3453.339	3446.764	0.001907586
9	800	3493.806	3486.665	0.002048089
8	700	3529.806	3522.024	0.002209525
7	600	3561.307	3552.783	0.002399246
6	500	3588.295	3578.894	0.002626789
5	400	3610.792	3600.315	0.002910023
4	300	3628.883	3617.011	0.003282268
3	200	3642.82	3628.956	0.003820383
2	100	3653.579	3636.131	0.004798507
1	0	3655.973	3638.524	0.004795626

Table 7. The data of the Earth planet of the new earth model.

Level	Radius	Density	Mass of shell	Moment of Inertia	Level	Radius	Density	Mass of shell	Moment of Inertia
No.	km	g/cm^3	10^{24} g	10^{40} g.cm^2	No.	km	g/cm^3	10^{24} g	10^{40} g.cm^2
94	6371.0	1.02000			47	4000.0	5.30724	108.883	1190.942
93	6368.0	1.02000	1.560	42.192	46	3900.0	5.35706	104.551	1087.797
92	6368.0	2.60000	0.000	0.000	45	3800.0	5.40681	100.252	990.939
91	6356.0	2.60000	15.869	428.205	44	3700.0	5.45657	95.991	900.186
90	6356.0	2.90000	0.000	0.000	43	3630.0	5.49145	64.681	579.291
89	6346.6	2.90000	13.818	371.612	42	3630.0	5.49145	0.000	0.000
88	6346.6	3.38076	0.000	0.000	41	3600.0	5.50642	27.091	236.031
87	6331.0	3.37906	26.623	713.154	40	3500.0	5.55641	87.605	736.274
86	6311.0	3.37688	33.921	903.543	39	3480.0	6.56645	17.025	138.243
85	6291.0	3.37471	33.885	891.587	38	3400.0	5.60987	66.482	524.600
84	6291.0	3.37471	0.000	0.000	37	3300.0	5.66415	79.503	595.032
83	6256.0	3.37091	58.383	1531.873	36	3200.0	5.71843	75.548	532.191
82	6221.0	3.36710	57.669	1496.283	35	3100.0	5.77270	71.647	474.147
81	6186.0	3.36330	56.960	1461.353	34	3000.0	5.82698	67.805	420.694
80	6151.0	3.35950	56.254	1427.019	33	2900.0	5.88126	64.026	371.635
79	6151.0	3.43578	0.000	0.000	32	2800.0	5.93553	60.313	326.765
78	6106.0	3.46264	73.258	1834.339	31	2700.0	5.98981	56.671	285.875
77	6061.0	3.48951	72.748	1794.926	30	2600.0	6.04409	53.104	248.764
76	6016.0	3.51639	72.230	1755.876	29	2500.0	6.09837	49.616	215.223
75	5971.0	3.54325	71.702	1717.172	28	2400.0	6.15264	46.211	185.049
74	5971.0	3.72378	0.000	0.000	27	2300.0	6.20692	42.893	158.036
73	5921.0	3.78678	83.421	1966.289	26	2200.0	6.26120	39.666	133.982
72	5871.0	3.84980	83.400	1932.878	25	2100.0	6.31547	36.534	112.688
71	5821.0	3.91282	83.344	1898.957	24	2000.0	6.36975	33.502	93.955
70	5771.0	3.97584	83.256	1864.631	23	1900.0	6.42403	30.573	77.588
69	5771.0	3.97584	0.000	0.000	22	1800.0	6.47831	27.752	63.398
68	5736.0	3.98399	57.945	1278.777	21	1787.5	6.48509	3.276	7.027
67	5701.0	3.99214	57.359	1250.499	20	1700.0	6.52703	21.757	44.150
66	5701.0	4.38071	0.000	0.000	19	1600.0	6.88649	22.952	41.722
65	5650.0	4.41241	90.762	1949.III	18	1500.0	7.03784	21.027	33.736
64	5600.0	4.44316	88.027	1856.879	17	1400.0	7.09459	18.677	26.231
63	5600.0	4.44317	0.000	0.000	16	1300.0	7.15135	16.321	19.875
62	5500.0	4.50372	173.161	3556.332	15	1221.5	7.17442	11.235	11.924
61	5400.0	4.56307	169.215	3351.201	14	1221.5	9.17442	0.000	0.000
60	5300.0	4.62129	165.176	3152.302	13	1200.0	9.18575	3.636	3.554
59	5200.0	4.67844	161.058	2959.895	12	1100.0	9.23583	15.317	13.547
58	5100.0	4.73460	156.869	2774.141	11	1000.0	9.28155	12.837	9.471
57	5000.0	4.78983	152.621	2595.240	10	900.0	9.32293	10.560	6.383
56	4900.0	4.84422	148.325	2423.294	9	800.0	9.35994	8.491	4.113
55	4800.0	4.89783	143.989	2258.383	8	700.0	9.39260	6.638	2.507
54	4700.0	4.95073	139.623	2100.552	7	600.0	9.42091	5.004	1.423
53	4600.0	5.00299	135.234	1949.779	6	500.0	9.44486	3.596	0.735
52	4500.0	5.05469	130.833	1806.076	5	400.0	9.46446	2.416	0.333
51	4400.0	5.10590	126.426	1669.385	4	300.0	9.47970	1.468	0.124
50	4300.0	5.15669	122.021	1539.631	3	200.0	9.49059	0.755	0.034
49	4200.0	5.20713	117.625	1416.725	2	100.0	9.49712	0.278	0.005
48	4100.0	5.25729	113.243	1300.533	1	0.0	9.49821	0.040	0.000
Total								5,121.820	76,126.841
Insufficiency								852.380	4,159.559

Table 8. The data of the dark planet of the new earth model.

Le-vel	Radius R	Density ρ	Mass of shell ΔM	Moment of Inertia ΔI		Le-vel	Radius R	Density ρ	Mass of shell ΔM	Moment of Inertia ΔI
No.	km	g/cm^3	10^{24} g	10^{40} $g.cm^2$		No.	km	g/cm^3	10^{24} g	10^{40} $g.cm^2$
45	3700.375	2.70000								
44	3700.000	2.70053	0.174	1.590		22	1800.000	5.40184	22.932	52.388
43	3030.000	2.80006	32.497	291.052		21	1787.500	5.41961	2.7351	5.860
42	3030.000	2.80006	0.000	0.000		20	1700.000	6.64401	8.3321	37.199
41	3600.000	2.84271	13.900	121.102		19	1600.000	6.68619	9.2161	34.931
40	3500.000	2.98488	46.148	387.849		18	1500.000	6.82836	7.3881	27.897
39	3480.000	3.01332	9.181	74.550		17	1400.000	6.97063	6.6931	21.899
38	3400.000	3.12706	36.526	288.220		16	1300.000	6.11271	3.843	16.858
37	3300.000	3.26923	45.106	337.590		15	1221.500	6.22431	9.675	10.269
36	3200.000	3.41140	44.340	312.352		14	1221.500	6.22431	0.000	0.000
35	3100.000	3.55358	43.427	287.389		13	1200.000	6.25488	2.471	2.415
34	3000.000	3.69575	42.376	262.917		12	1100.000	6.39706	10.520	9.304
33	2900.000	3.83792	41.198	239.129		11	1000.000	6.53923	8.968	6.616
32	2800.000	3.98010	39.904	216.189		10	900.000	6.68140	7.604	4.536
31	2700.000	4.12227	38.504	194.231		09	800.000	6.82358	6.138	2.973
30	2600.000	4.26445	37.010	173.370		08	700.000	6.96676	4.881	1.844
29	2500.000	4.40662	35.431	153.693		07	600.000	7.10793	3.743	1.005
28	2400.000	4.54879	33.780	135.269		06	500.000	7.26010	2.736	0.559
27	2300.000	4.69097	32.066	118.145		05	400.000	7.39227	1.871	0.258
26	2200.000	4.83314	30.300	102.346		04	300.000	7.63445	1.167	0.098
25	2100.000	4.97532	28.493	87.885		03	200.000	7.67662	0.605	0.027
24	2000.000	5.11749	26.655	74.754		02	100.000	7.81880	0.227	0.004
23	1900.000	5.25966	24.798	62.933		01	0.000	7.96097	0.033	0.000
Total									852.380	4,159.559

Table 9. The global data of the new Earth model.

Level	Radius	Density	Mass of shell	Mass Within Radius	Moment of Inertia	Moment within Radius	Pressure	Gravity
No.	km	g/cm^3	10^{24} g	10^{24} g	10^{40} $g.cm^2$	10^{40} $g.cm^2$	kbar	cm/s^2
94	6371.0	1.02000		5974.200		80286.400	0.000	982.108
93	6368.0	1.02000	1.560	5972.640	42.192	80244.208	0.301	982.778
92	6368.0	2.60000	0.000	5972.640	0.000	80244.208	0.301	982.778
91	6356.0	2.60000	15.869	5956.771	428.205	79816.003	3.369	983.871
90	6356.0	2.90000	0.000	5956.771	0.000	79816.003	3.369	983.871
89	6346.6	2.90000	13.818	5942.953	371.612	79444.391	6.051	984.499
88	6346.6	3.38076	0.000	5942.953	0.000	79444.391	6.051	984.499
87	6331.0	3.37906	26.623	5916.330	713.154	78731.237	11.244	984.924
86	6311.0	3.37688	33.921	5882.409	903.543	77827.694	17.900	985.494
85	6291.0	3.37471	33.885	5848.724	891.587	76936.107	24.555	986.091
84	6291.0	3.37471	0.000	5848.724	0.000	76936.107	24.555	986.091
83	6256.0	3.37091	58.383	5790.341	1531.873	75404.234	36.203	987.201
82	6221.0	3.36710	57.669	5732.672	1496.283	73907.952	47.850	988.398
81	6186.0	3.36330	56.960	5675.712	1461.353	72446.598	59.500	989.682
80	6151.0	3.35950	56.254	5619.458	1427.019	71019.579	71.151	991.056
79	6151.0	3.43578	0.000	5619.458	0.000	71019.579	71.151	991.056
78	6106.0	3.46264	73.258	5546.201	1834.339	69185.240	86.546	992.606
77	6061.0	3.48951	72.748	5473.453	1794.926	67390.314	102.086	994.187
76	6016.0	3.51639	72.230	5401.223	1755.876	65634.438	117.771	995.799
75	5971.0	3.54325	71.702	5329.521	1717.172	63917.266	133.601	997.445
74	5971.0	3.72378	0.000	5329.521	0.000	63917.266	133.601	997.445
73	5921.0	3.78678	83.421	5246.099	1966.289	61950.978	152.340	998.485
72	5871.0	3.84980	83.400	5162.699	1932.878	60018.100	171.412	999.419
71	5821.0	3.91282	83.344	5079.354	1898.957	58119.143	190.816	1000.250
70	6771.0	3.97584	83.256	4996.099	1864.631	56254.512	210.551	1000.977
69	5771.0	3.97584	0.000	4996.099	0.000	56254.512	210.551	1000.977
68	5736.0	3.98399	57.945	4938.154	1278.777	54975.735	224.498	1001.478
67	5701.0	3.99214	57.359	4880.795	1250.499	53725.236	238.480	1002.036
66	5701.0	4.38071	0.000	4880.795	0.000	53725.236	238.480	1002.036
65	5650.0	4.41241	90.762	4790.033	1949.111	51776.126	260.941	1001.237
64	5600.0	4.44316	88.027	4702.006	1856.879	49919.246	283.099	1000.466
63	5600.0	4.44317	0.000	4702.006	0.000	49919.246	283.099	1000.466
62	5500.0	4.50372	173.161	4528.845	3556.332	46362.914	327.829	998.981
61	5400.0	4.56307	169.215	4359.630	3351.201	43011.713	373.094	997.602
60	5300.0	4.62129	165.176	4194.454	3152.302	39859.411	418.886	996.366
59	5200.0	4.67844	161.058	4033.396	2959.895	36899.516	465.200	995.312
58	5100.0	4.73460	156.869	3876.527	2774.141	34125.375	512.034	994.483
57	5000.0	4.78983	152.621	3723.905	2595.240	31530.135	559.390	993.925
56	4900.0	4.84422	148.325	3575.581	2423.294	29106.841	607.272	993.687
55	4800.0	4.89783	143.989	3431.592	2258.383	26848.458	655.688	993.821
64	4700.0	4.95073	139.623	3291.969	2100.552	24747.907	704.651	994.386
53	4600.0	5.00299	135.234	3156.734	1949.779	22798.128	754.177	995.445
52	4500.0	5.05469	130.833	3025.901	1806.076	20992.051	804.289	997.068
51	4400.0	5.10590	126.426	2899.475	1669.385	19322.667	855.012	999.330
50	4300.0	5.15669	122.021	2777.455	1539.631	17783.035	906.379	1002.317
49	4200.0	5.20713	117.625	2659.830	1416.725	16366.310	958.429	1006.122
48	4100.0	5.25729	113.243	2546.587	1300.533	15065.777	1011.207	1010.848

Level	Radius	Density	Mass of shell	Mass Within Radius	Moment of Inertia	Moment within Radius	Pressure	Gravity
No.	km	g/cm^3	10^{24} g	10^{24} g	10^{40} $g.cm^2$	10^{40} $g.cm^2$	kbar	cm/sec^2
47	4000.0	5.30724	108.883	2437.704	1190.942	13874.835	1064.767	1016.614
46	3900.0	5.35706	104.551	2333.152	1087.797	12787.039	1119.172	1023.550
45	3800.0	5.40681	100.252	2232.900	990.939	11796.100	1174.494	1031.804
44	3700.0	5.45657	96.165	2136.734	901.775	10894.325	1230.814	1041.459
43	3630.0	5.49145	97.178	2039.557	870.342	10023.983	1270.565	1032.803
42	3630.0	5.49145	0.000	2039.557	0.000	10023.983	1270.565	1032.803
41	3600.0	5.50642	40.991	1998.565	357.133	9666.850	1287.573	1028.983
40	3500.0	5.55641	133.753	1864.812	1124.123	8542.727	1344.157	1015.767
39	3480.0	5.56645	26.206	1838.606	212.793	8329.934	1355.440	1013.037
38	3400.0	5.60987	103.008	1735.599	812.820	7517.114	1400.496	1001.813
37	3300.0	5.66415	124.609	1610.990	932.622	6584.492	1456.591	987.097
36	3200.0	5.71843	119.888	1491.103	844.543	5739.949	1512.369	971.634
35	3100.0	5.77270	115.074	1376.028	761.536	4978.413	1567.772	955.430
34	3000.0	5.82698	110.181	1265.847	683.611	4294.802	1622.740	938.499
33	2900.0	5.88126	105.224	1160.623	610.764	3684.038	1677.213	920.853
32	2800.0	5.93553	100.217	1060.406	542.954	3141.084	1731.131	902.508
31	2700.0	5.98981	95.175	965.230	480.106	2660.978	1784.433	883.483
30	2600.0	6.04409	90.114	875.116	422.134	2238.844	1837.060	863.802
29	2500.0	6.09837	85.047	790.069	368.916	1869.928	1888.951	843.490
28	2400.0	6.15264	79.991	710.079	320.318	1549.610	1940.047	822.582
27	2300.0	6.20692	74.959	635.120	276.181	1273.429	1990.291	801.116
26	2200.0	6.26120	69.966	565.154	236.328	1037.100	2039.628	779.142
25	2100.0	6.31547	65.027	500.126	200.573	836.527	2088.003	756.721
24	2000.0	6.36975	60.157	439.969	168.709	667.819	2135.368	733.934
23	1900.0	6.42403	55.371	384.598	140.521	527.298	2181.678	710.878
22	1800.0	6.47831	50.684	333.914	115.786	411.511	2226.896	687.677
21	1787.5	6.48509	6.011	327.903	12.893	398.618	2232.456	684.776
20	1700.0	6.52703	40.089	287.814	81.349	317.269	2270.939	664.522
19	1600.0	6.88649	42.168	245.646	76.653	240.617	2314.824	640.272
18	1500.0	7.03784	38.415	207.231	61.633	178.984	2358.655	614.564
17	1400.0	7.09459	34.270	172.961	48.130	130.854	2401.336	588.826
16	1300.0	7.15135	30.164	142.798	36.733	94.121	2442.566	563.807
15	1221.5	7.17442	20.910	121.888	22.193	71.928	2473.835	545.091
14	1221.5	9.17442	0.000	121.888	0.000	71.928	2473.835	545.091
13	1200.0	9.18575	6.107	115.781	5.969	65.959	2484.512	536.500
12	1100.0	9.23583	25.837	89.944	22.851	43.108	2532.405	496.000
11	1000.0	9.28155	21.805	68.139	16.087	27.021	2576.798	454.664
10	900.0	9.32293	18.064	50.076	10.919	16.102	2617.562	412.515
9	800.0	9.35994	14.629	35.447	7.086	9.016	2654.582	369.568
8	700.0	9.39260	11.519	23.928	4.351	4.665	2687.749	325.841
7	600.0	9.42091	8.747	15.181	2.488	2.176	2716.972	281.380
6	500.0	9.44486	6.332	8.850	1.294	0.882	2742.182	236.210
5	400.0	9.46446	4.287	4.563	0.591	0.291	2763.336	190.294
4	300.0	9.47970	2.625	1.938	0.222	0.069	2780.457	143.683
3	200.0	9.49059	1.360	0.578	0.061	0.009	2793.727	96.419
2	100.0	9.49712	0.505	0.073	0.009	0.000	2804.037	48.710
1	0.0	9.49821	0.073	0.000	0.000	0.000	2805.297	0.000

從弦論的時空探究地球內部的暗物質

新思潮研究室
何 顯 榮

摘 要

暗物質困擾科學家已八十餘年，至今仍無所獲，嘗試應用十維時空的弦論解決問題。根據「因果論」和「人本原理」可以將大宇宙分成三重宇宙，而暗物質就是其他宇宙空間的星球。為解決暗物質的研究瓶頸，最好的方法是從我們生存其間的地球開始。分析地球內部深處的構造、溫度、密度和壓力，探究地球內部組成。根據分析結果推論，地函下層和外核上層的化學成分相似，僅是固態岩石和液態岩漿的物態變化而已，兩者之間密度分布應呈連續性。在外核低黏滯性的Ｆ層，組成岩漿的各種氧化物和較活潑的金屬元素，產生氧化還原化學反應和重力分離作用，被還原的重金屬沉澱於內核面。大量的氧化還原化學反應熱、放射性元素衰變產生的輻射熱，以及地心核分裂熱，成為從外核Ｆ層到地殼之間一貫性大對流囊的主要動力源。根據這個地球新模式，應用簡化法計算，求得地球的質量是5121.82 $\times 10^{24}$ g和轉動慣量是76126.841 $\times 10^{40}$ g.cm^2,只有地球科學家實際觀測值的85.73％和94.82 ％。引用多重宇宙的結構，解決上述質量和轉動慣量的不足值。擬定一些合理的假設，計算出地球有一暗物質的行星，存在於地球內部我們看不見的另一重宇宙中，其半徑有3700.375公里，約為火星的1.33倍。本研究的新地球模式，或可引用錢德勒擺動做為佐證，並且可以初步解釋一些科學上的問題，例如暗物質、暗能量和地球組成等問題。